LATVIJAS UNIVERSITĀTE
FIZIKAS UN MATEMĀTIKAS FAKULTĀTE

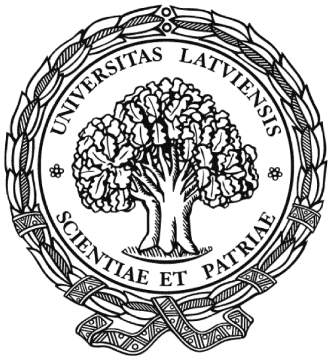

Dmitrijs Bočarovs

VIRSMAS ĪPAŠĪBU UN REAKCIJAS SPĒJU MODELĒŠANA NO PIRMAJIEM PRINCIPIEM NITRĪDU KODOLU DEGVIELAI

Promocijas darbs

Doktora zinātniskā grāda iegūšanai fizikā

Apakšnozare: cietvielu fizika

Promocijas darba vadītājs: *Dr. chem.* **Jurijs Žukovskis**

Rīga, 2012

Promocijas darbs izstrādāts no 2006. gada oktobra līdz 2011. gada augustam
Latvijas Universitātes Cietvielu fizikas institūtā.

Darba forma: publikāciju kopa.

Šis darbs izstrādāts ar Eiropas Sociālā fonda atbalstu projekta „Datorzinatnes pielietojumi un tās saiknes ar kvantu fiziku".
Līguma Nr. 2009/0216/1DP/1.1.1.2.0/09/APIA/VIAA/044

IEGULDĪJUMS TAVĀ NĀKOTNĒ

Promocijas darba vadītājs:
Dr. chem. LU Cietvielu fizikas institūta vadošais petnieks **Jurijs Žukovskis**

Promocijas darba recenzenti:
Dr. lektors **Ģirts Barinovs,** Latvijas Universitātes Fizikas un matemātikas fakultāte
Dr. prof. **Roberto Kačufo** *(Roberto Caciuffo),* Eiropas Komisijas Transurāna elementu institūts
Dr. habil. vadošais pētnieks **Linards Skuja,** Latvijas Universitātes Cietvielu fizikas institūts

Promocijas darbs tiks aizstāvēts atklātā sesijā
LU Fizikas, astronomijas un mehānikas specializētajā promocijas padomes sēdē 2012. gada 24. janvārī. plkst. 15.00 Cietvielu fizikas institūtā Ķengaraga ielā 8, Rīgā.

Ar darbu un tā kopsavilkumu var iepazīties Latvijas Universitātes Bibliotēkā Rīgā, Kalpaka bulv. 4, un Latvijas Akadēmiskajā bibliotēkā Rīgā, Rūpniecības ielā 10.

LU Fizikas un astronomijas zinātnes nozares specializētās promocijas padomes priekšsēdētājs: *Dr. habil. phys.* **Ivars Tāle**

Anotācija

Urāna mononitrīds UN ir viens no materiāliem, kuru var izmantot kā perspektīvu degvielu IV paaudzes kodolu reaktoriem. Tā kā UN paraugos vienmēr atrodas ievērojams daudzums skābekļa piemaisījumu, nepieciešams izprast O adsorbcijas mehānismu, kā arī tam sekojošo UN oksidēšanos.

Mēs pirmo reizi veicām UN virsmas un tās mijiedarbības ar skābekli detalizētu pētījumu, izmantojot DFT PAW metodi *VASP* programmas ietvaros. U un N vakances veidošanās enerģijas, kā arī saites enerģijas virs UN virsmas adsorbētajiem skābekļa atomiem un molekulām tika apskatītas kopā ar lādiņu pārdalīšanos, elektronisko stāvokļu blīvumu un O atomu migrācijas trajektorijām. Veiktie aprēķini ļauj piedāvāt enerģētiski iespējamo mehānismu UN(001) virsmas daļējai piesātināšanai ar skābekli. Tas izskaidro eksperimentāli novērojamo vieglo UN oksidāciju gaisā.

Atslēgvārdi: kvantu ķīmija, blīvuma funkcionāļa teorijas aprēķini, urāna mono- nitrīds, virsmas defekti, skābekļa adsorbcija.

Abstract

The uranium mononitride UN is a material considered as promising candidate for Generation-IV nuclear reactors. Due to considerable amount of aggressive oxygen impurities in UN samples, it is necessary to understand the mechanism of O adsorption and further oxidation of UN.

The first detailed study of UN surface, including its interaction with oxygen, have been performed using DFT PAW method as implemented in the *VASP* computer code. The formation energies of U and N vacancies as well as binding energies of O atoms and molecules adsorbed atop the UN surface are discussed together with the charge redistributions, densities of states, and O atom migration trajectories. Calculations allow us to propose energetically feasible mechanism for the partial saturation of UN(001) surface by oxygen which can lead to easy UN oxidation observed in air.

Keywords: Quantum chemistry, Density Functional Theory calculations, uranium mononitride, surface defects, oxygen adsorption

Autora publicētie darbi par promocijas tēmu

[P1] R.A. Evarestov, A.V. Bandura, M.V. Losev, E.A. Kotomin, Yu.F. Zhukovskii, and D. Bocharov, A first principles DFT study in UN bulk and (001) surface: Comparative LCAO and PW calculations. - J. Comput. Chem., 2008, **29**, p. 2079-2087.

[P2] Yu.F. Zhukovskii, D. Bocharov, E.A. Kotomin, R.A. Evarestov, and A.V. Bandura, First principles calculations of oxygen adsorption on the UN(001) surface. - Surf. Sci., 2009, **603**, p. 50-53.

[P3] Yu.F. Zhukovskii, D. Bocharov, and E.A. Kotomin, Chemisorption of a molecular oxygen on the UN (001) surface: *ab initio* calculations. - J. Nucl. Mater., 2009, **393**, p. 504-507.

[P4] D. Bocharov, D. Gryaznov, Yu.F. Zhukovskii, and E.A. Kotomin, DFT calculations of point defects on UN(001) surface. - Surf. Sci., 2011, **605**, p. 396-400.

[P5] D. Bocharov, D. Gryaznov, Yu.F. Zhukovskii, E.A. Kotomin, *Ab initio* modeling of oxygen impurity atom incorporation into uranium mononitride surface and subsurface vacancies. - J. Nucl. Mater., 2011, **416**, p. 200-204.

A First-Principles DFT Study of UN Bulk and (001) Surface: Comparative LCAO and PW Calculations

R. A. EVARESTOV,[1] A. V. BANDURA,[1] M. V. LOSEV,[1] E. A. KOTOMIN,[2] Yu. F. ZHUKOVSKII,[2] D. BOCHAROV[2]
[1]*Department of Quantum Chemistry, St. Petersburg State University, 198504 St. Peterhof, University Prospect 26, Russia*
[2]*Institute for Solid State Physics, University of Latvia, 8 Kengaraga Str., Riga, LV-1063, Latvia*

Received 13 January 2008; Revised 10 April 2008; Accepted 11 April 2008
DOI 10.1002/jcc.21023
Published online 21 May 2008 in Wiley InterScience (www.interscience.wiley.com).

Abstract: LCAO and PW DFT calculations of the lattice constant, bulk modulus, cohesive energy, charge distribution, band structure, and DOS for UN single crystal are analyzed. It is demonstrated that a choice of the uranium atom relativistic effective core potentials considerably affects the band structure and magnetic structure at low temperatures. All calculations indicate mixed metallic-covalent chemical bonding in UN crystal with U5*f* states near the Fermi level. On the basis of the experience accumulated in UN bulk simulations, we compare the atomic and electronic structure as well as the formation energy for UN(001) surface calculated on slabs of different thickness using both DFT approaches.

 J Comput Chem 29: 2079–2087, 2008

Key words: first-principles calculations; actinides; uranium nitride

Introduction

Uranium mononitride and carbide (UN, UC) attract a considerable attention as promising nuclear fuel materials for novel Generation IV reactors.[1] In particular, nitrides and carbides exhibit higher thermal conductivity, melting temperature, and metal density when compared with uranium dioxide that is commonly used nowadays. To predict nuclear fuel performance under different operating conditions and then a prolonged time in repository for used fuel, it is necessary to understand and predict material physicochemical properties. Of special importance are surface properties because commercial fuels are used as powders and UN, UC are effectively oxidized in air. The more so, numerous grain boundaries considerably affect material properties.

Theoretical studies of uranium compounds are difficult due to a relativistic character of electron motion in the U atom core and strong electron–electron correlation. Moreover, UN is a rather complicated system because it is characterized by a mixed metal-covalent chemical bonding. The metallic part (U5*f* states near the Fermi level) is better described by a delocalized basis of the Plane Waves (PW), whereas the covalent part (U5*f*-N2*p* hybridization) by a Linear Combination of Atomic Orbital (LCAO) basis set. This is why in this article we compare results of both approaches.

In Section "Previous *ab initio* simulations on UN bulk," the comparison is made for the bulk properties (studied earlier experimentally), with a detailed analysis of relativistic pseudopotentials in Section "Current DFT LCAO and PW calculations on UN bulk." In "DFT LCAO and PW calculations on UN(001) surface" section, we discuss—for the first time—the (001) surface properties (so far, the atomistic simulations on U compound substrates were performed only for densely packed UO_2 surfaces[2]).

Previous *Ab Initio* Simulations on UN Bulk

UN single crystal possesses *fcc* (face-centered cubic) structure with two atoms per unit cell: the lattice constant $a_0 = 4.886$ Å, the bulk modulus $B = 194$ GPa, and the cohesive energy $E_0 = 13.6$ eV.[1] These properties could be used as the test for theoretical calculations. Below 53 K UN undergoes the antiferromagnetic (AFM) ordering with the doubled unit cell and the spin density (SD) of 0.75 μ_B per U ion (at 4.2 K). Above this temperature, it reveals paramagnetic properties with the effective magnetic moment in the Curie-Weiss law of $\sim$3.1 μ_B. UN shows a metallic conductivity.

So far, most of calculations were performed for the high temperature phase (a primitive unit cell) relevant for fuel applications. The first relativistic KKR[3] and LMTO[4] calculations were performed already in 80s focusing mostly on the atomic and band structure of UN crystal. The calculated lattice parameters were within 3% of the experimental value, whereas the bulk

Correspondence to: R. A. Evarestov; e-mail: re1973@re1973.spb.edu

Table 1. Calculated Properties of UN Bulk Crystal.[a]

Property	PBE-AE-LAPW[5,6 b]	PBE-US[9]	PW91-PAW[10 c]	PW91-US[11 d]	PW91-AE[12]	PW91-LCAO[13 e]
a_0, Å	4.886	4.820	4.864	4.954	4.90	Fixed expt.
B, GPa	209		226	182		
E_c, eV	13.4		14.7	12.3		9.9–12.8
SD, μ_B	1.25		1.05			3.02–3.20

Lattice constant a_0, bulk modulus B, cohesive energy E_c and spin density SD per unit cell. AE, all electrons; US, ultrasoft pseudopotentials.
[a]In the LCAO approach, the value of E_c is calculated with respect to the free N and U atoms, whereas in the PW approach it was estimated with respect to the same atoms placed in cubic supercells with large (10 Å) translation vectors.
[b]WIEN-2k code.
[c]VASP code.
[d]CASTEP code.
[e]GAUSSIAN code.

modulus was reproduced worse, within 11%. Only recently these first principles calculations were continued (Table 1). In particular, the all-electron (AE) LAPW calculations (refs. 5, 6; Sedmidubsky et al., unpublished, 2005) were performed using the GGA-PBE (Perdew-Burke-Ernzerhof) exchange correlation functionals with and without incorporation of the spin-orbital interaction (WIEN-2k computer code) for a series of actinide nitrides. The calculated cohesive energy and the lattice constant are close to the experimental values. Incorporation of the spin-orbital coupling leads to a large (8.2 eV) splitting of U*6p* semicore into $6p_{1/2}$ and $6p_{3/2}$ as well as slight reduction of the magnetic moment from 1.25 down to 1.16 μ_B. The hybridization of N*2p*, U*5f*, and U*6d* states was observed in the Brillouin zone (BZ) due to their overlap: the N*2p* energy levels lie in the region of -6 to -1 eV whereas the U*5f* states dominate near and at the Fermi level. The calculated band structure around the Fermi level is in qualitative agreement with the experimental UPS spectra.[7,8]

In ref. 6 the WIEN-2k calculations were complemented by a study of the AFM phase. The lattice constant is in a good agreement with the experiment (~0.4%), but—unlike the experiment—the ferromagnetic structure is found to be lower in energy, with the SD = 0.96 μ_B. It should be pointed out that this is presumably a failing of the PBE functional. Notice, that due to use of muffin-tin spheres, the attribution of the electronic and spin density to individual ions is not uniquely defined.

Systematic DFT-PW calculations were also performed, starting with a study[9] focused on the UN and UC atomic structure. Using the ultra-soft (US) pseudopotentials and PBE96 exchange-correlation functional, the experimental UN and U_2N_3 lattice constants were reproduced within 3% error. In the more detailed UN, UN_2, and U_2N_3 DFT PW calculations, the VASP[10] and CASTEP[11] codes using the Perdew-Wang (PW91) nonlocal GGA exchange-correlation functional[14] were employed and combined with either the US or PAW pseudopotentials, respectively. Both methods agree on complicated mixed metallic-covalent nature of the UN chemical bonding and reproduce well the lattice constants, bulk moduli, and cohesive energies. Analogously to previous calculations for the primitive unit cell, they suggest the magnetic moment on U ion close to unity. The DFT PW approach combined with a supercell model was further used in the calculations of defective UN crystal, containing single point defects and Frenkel and Schottky defect pairs.[10,11] A study of defect properties is of key importance for the prediction of fuel behavior under operational conditions and in further centuries-long depository.

One more first-principles all-electron relativistic DFT study with GGA PW91 exchange correlation functional and numerical double ξ basis set was performed recently for UN and UN_2[12]; the results are compared with the experimental EXAFS and X-ray diffraction data. New element in that article is a calculation of the phonon frequencies and heat capacities, which are important for the fuel behavior prediction. Authors provide additional evidence for an important role of itinerant U*5f* states in thermodynamic properties.

To understand better the UN fuel performance, careful study of the chemical bonding in crystalline bulk and its surface properties is a necessary step. The LCAO approach is a natural way for such a study as it extends for the periodic systems the chemical bonding analysis developed in quantum chemistry of molecules,[15] and it is free of muffin-tin approximation problems. In particular, recent first principles DFT and hybrid HF-DFT LCAO calculations of UO_2 crystal[16] provided the structural, electronic, and magnetic properties in a good agreement with the experimental data.

The ground state valence electronic configurations of U and N atoms are $5f^3 6d^1 7s^2$ and $2s^2 2p^3$, respectively. In a crude ionic bonding picture, the U*6d* and *7s* electrons fill the N*2p* states and the three U*5f* electrons form the highest occupied molecular orbital (HOMO).[17] The LCAO calculations allow one to study this qualitative picture in more detail, analyzing the changes of the free atom electronic structure due to the chemical bonding formation, and to connect the energy bands of a solid with the atomic states. However, the first LCAO electronic structure calculations of crystalline UN have been only recently performed.[13] In that article, several different Relativistic Effective Core Potentials (RECP) containing 60, 78, and 81 electrons in a U ion core, which are discussed in more detail in the next RECP Formalism, were used and compared. In particular, for the RECP78, there exist 14 outermost uranium atom electrons

included into the valence shell ($6s^26p^66d^15f^37s^2$). The results obtained were compared with those for RECP60, where 32 outermost uranium atom electrons are included in the valence shell (the configuration $5s^25p^65d^{10}6s^26p^66d^15f^37s^2$). Lastly, in the RECP81 U5*f* electrons are included into the atomic core.

Recent LCAO calculations on UN bulk[13] have been performed using the GAUSSIAN-03 computer code with the PW91 exchange-correlation functional and periodic boundary conditions. Unlike previous PW calculations, the LCAO (RECP78) suggests the ground state with the three unpaired electrons ($S_z = 3/2$, i.e., $SD \approx 3\ \mu_B$) whereas the $S_z = 1/2$ state lies slightly higher in energy (~0.5 eV). The latter is close to that experimentally observed. The values of cohesive energy calculated for RECP78 and RECP60 considerably differ (9.86 and 12.8 eV, respectively, last column in Table 1), thus indicating an importance of the U outer shell relaxation.

Group-theoretical analysis performed for interpretation of the UN band structure demonstrates that threefold degenerate (at Γ point) U5*f* t_{2u} state is split at X and W points of the BZ due to hybridization with the N2*p* states, which produces a narrow band near the Fermi level (~2 eV). This band is occupied with 3 spin-up electrons. The U5*f* t_{1u} state is allowed by symmetry to mix up with N2*p* state at the Γ point and form a broad band to the lower-energy side. Lastly, the nondegenerate U5*f* a_{2u} state is empty; it forms the bottom of the conduction band (CB). In other words, both bottom of the CB and the top of the valence band (VB) are formed by U5*f* states which leads to the metallic nature of this compound[13] (unlike UO_2 which is a semiconductor[16]). The Mulliken effective atomic charges of ±(1.5–2.0) *e* calculated using the GAUSSIAN-03 code confirm the mixed nature of the UN chemical bonding and are in agreement with the Bader topological charges of ±1.6 *e* obtained in PW calculations.[11]

Current DFT LCAO and PW Calculations on UN Bulk

RECP Formalism

As mentioned above, the proper choice of relativistic core pseudopotentials is important for reliable DFT calculations. The different methods for construction of RECP have been suggested so far.[15] To the best of our knowledge, the small core (SC) pseudopotentials of U atom (60 core electrons, with 5*s*, 5*p*, and 5*d* electrons referred to the valence shell) were generated only for LCAO calculations. Unreliability of the large core (LC) pseudopotentials RECP78 for U was known in calculations of uranyl UO_2^{+2} ion[18] as well as molecules of uranium fluorides UF_5 and UF_6.[19] In particular, the most famous molecular failure was that for the uranyl ion, predicted to be bent using the LC RECP, whereas the correct linear structure was recovered only with the SC pseudopotential.

We use here the energy-adjusted small core (SC) pseudopotential by Stuttgart-Cologne group (SC60).[20] Its parameters are fitted to the excitation and ionization energies obtained in the relativistic all-electron calculations performed using a numerical finite difference approach. The RECP generation method based on numerical Dirac-Hartree-Fock wave function, allows one the computation of averaged (over $(l-1/2)$ and $(l+1/2)$ components) relativistic effective potentials (AREP) and includes also the effective spin-orbit potential (ESOP) operators. Use of the energy-adjusted pseudopotentials SC60 in the complete form (with ESOP) requires use of a two-component spinor (spin-orbital) formalism in molecular or crystalline calculations. In our scalar-relativistic calculations only the AREP part of RECP has been employed.

The accuracy of the calculations with the energy-adjusted RECPs is essentially limited by the demand that only the radially local (semilocal) RECP operator is used. A more strict treatment of the outermost core electrons (for example, U6*s* and 6*p* electrons) demands to treat them explicitly. Since effective potentials are somewhat different for the outermost core and valence electrons with the same orbital and total moment, new terms with projectors on the outermost core pseudoorbitals were added to the conventional core pseudopotential operator in the Generalized RECP (GRECP) method (see ref. 21 and references herein). The importance of additional nonlocal terms in the expression GRECP operator is demonstrated in U atom calculations.[22] In the present calculations we have used for U atom the only radially local AREP version by the Mosyagin-Titov LC (MT78) and SC (MT60) pseudopotentials.[13]

The radially local AREP form used in LCAO calculations is a sum of a Coulomb term *C*, a local term V_{loc} and a semilocal term V_{sl} usually presented analytically as

$$V_{PS}(\mathbf{r}) = C + V_{loc} + V_{sl} = -\frac{Z_N}{r} + \sum_{k=1}^{M} r^{n_k-2} C_k \exp(-\alpha_k r^2) + \sum_{l=0}^{3}\left[\sum_{k=1}^{M_l} r^{n_{kl}-2} C_{kl} \exp(-\alpha_{kl} r^2)\right]\hat{P}_l \quad (1)$$

where Z_N in a Coulomb term is the effective nuclear charge (total nuclear charge minus the number of electrons represented by RECP); n_k, n_{kl} = 0, 1, 2 and C_k, C_{kl}, α_k, α_{kl} are fitting parameters. The local term is a sum of products of polynomial and Gaussian radial functions whereas a semilocal term contains a sum of products of polynomial radial functions, Gaussian radial functions and angular momentum projection operators $\hat{P}_l$. Therefore, to specify the semilocal RECP, one needs to include a set of triplets (coefficient, power of *r* and exponent) for each term in each angular momentum of RECP. The contraction coefficients C_k, C_{kl}, exponents α_k, α_{kl} and powers n_k, n_{kl} are found by fitting the numerical AREP to expansions in Gaussian type functions (GTF) for the different RECP versions.

For each AREP the corresponding numerical atomic orbitals are approximated by the GTFs linear combinations, including both contracted and primitive GTOs. In particular, the contracted part of a U basis set (12*s*11*p*10*d*8*f*)/(8*s*7*p*6*d*4*f*) corresponding to the RECP SC60 in the segmented contraction scheme, defines three *s*-type (5*s*, 6*s*, 7*s*), two *p*-type (5*p*, 6*p*), two *d*-type (5*d*, 6*d*) and one *f*-type (5*f*) orbitals, occupied by the valence electrons in the ground state of U atom. The rest (primitive) GTOs are polarizing and diffuse orbitals necessary to properly describe the tails of the free-atom wave functions. The basis sets 11*s*5*p*6*d*5*f* and 6*s*3*p*4*d*4*f* have been used in our MT60 and MT78 RECP calculations, respectively. Table 2 presents the diffuse primitive Gaus-

Table 2. Diffuse Primitive Gaussian Exponents in the Basis Set of a Free U Atom Corresponding to the Stuttgart-Cologne Pseudopotential SC60.[18]

	Shell type			
GTO	*s*	*p*	*d*	*f*
1	0.071170	0.005000	0.073273	0.181420
2	0.030539		0.005000	0.005000
3	0.005000			

sian exponents in the basis set of a free U atom corresponding to the SC60 pseudopotential.

It is well known that for LCAO bulk calculations the basis set (BS) of free atom has to be modified as the diffuse functions cause numerical problems because of the large overlap with the core functions of the neighboring atoms in a dense-packed crystal.[15] This is why in the bulk calculations the diffuse exponents are either removed (as done in our calculations) or optimized, in order to minimize the total energy per unit cell. For example, the detailed BS optimization performed for Hartree-Fock (HF) and DFT LCAO calculations on $ATiO_3$ perovskites (A = Sr, Ba, Pb)[15] resulted in a good correlation with available experimental data (lattice parameters, bulk moduli and optical band gaps). Although there exist different algorithms for minimization of many-variables functions,[23,24] no analysis of their efficiency for the BS optimization in crystals was done so far.

In our PW calculations presented here the VASP code[25] was applied with the projector-augmented-wave (PAW) pseudopotentials for U and N atoms. The PAW method by Blöchl[26] uses the transformation operator between pseudo-orbitals and original orbitals combining the pseudopotential approach and LAPW method. The U PAW78 pseudopotential with a large U core (LC) RECP (78 core electrons, 14 valence electrons) is the same as in previous VASP calculations on UN[10,11] containing the closed shell configuration $6s^26p^65f^26d^27s^2$ while the U ground state possesses an open shell configuration known as $6s^26p^65f^36d^17s^2$.[25] Unlike those calculations, we have used here two different exchange-correlation functionals and very high accuracy in both *k*-point mesh and cut-off energy. Both LCAO and PW spin-polarized (FM) bulk calculations have been performed for the cubic crystalline structure of UN.

LCAO and PW Calculations on UN Bulk

Previous LCAO calculations clearly demonstrated that the chemical bonding in UN crystal has a metallic-covalent character.[13,17] The partly covalent bonds are formed by the interaction of U5*f* and 6*d* states with the N2*p* states. It was shown that the inclusion of 5*f* electrons in the atomic core (RECP81[13]) introduces small changes in the calculated cohesive energy of UN crystal and electron charge distribution. However, the inclusion of 5*s*, 5*p*, and 5*d* electrons in the valence shell results in a better agreement with values of both calculated and experimentally measured cohesion energy.

In the present and former[13] LCAO studies of UN bulk, we have used the two computer codes: the GAUSSIAN-03[27] and the CRYSTAL-06[28] suited for periodic systems. Both these codes give close results if the direct lattice summation is made up to 50 a.u. in the GAUSSIAN-03 and the tolerances 8 8 8 16 are used in CRYSTAL-06 for the Coulomb and exchange integrals calculations. The Monkhorst-Pack scheme[29] for 16 × 16 × 16 *k*-point mesh in the BZ was applied in both cases. For the N atom, the all-electron basis set 6-311++G(2*d*,2*p*)[30] was used, while the diffuse Gaussian function with the orbital exponent 0.0639 $a.u^{-1}$ was removed from the crystal calculation. As to BS of U atom, all diffuse orbitals (with orbital exponents less than 0.1 $a.u^{-1}$) were removed from the bulk calculations but retained in the free atom calculations.

The results of DFT-LCAO calculations on UN bulk using PW91 exchange and correlation functionals are presented in Table 3 for three different RECPs described above in RECP Formalism. Table 3 shows that the E_c is essentially underestimated in MT78 calculations, but is close to the experimental value in MT60 and SC60 calculations. As to the lattice parameter a_0, our LCAO DFT values (4.78 and 4.80 Å) do not differ much from those obtained in other DFT calculations (Table 1). The bulk modulus B is underestimated in MT78 calculations and overestimated both in MT60 and SC60 calculations. The calculated effective charge of U atom in UN (Q_U) is close to 1.6 *e* for all three RECP used and comparable to 1.7 *e* found in PW PAW78 calculations[10] using the topological Bader analysis.

Table 3 shows also that the populations of 6*d* and 5*f* orbitals on U atom are sensitive to the RECP choice. The AO populations allow us to analyze a role of different U atomic orbitals in the U-N chemical bonding using the RECP SC60 for a valence configuration $5s^25p^65d^{10}6s^26p^66d^15f^37s^2$. The conclusion could be drawn from the Table 3 that the sum of 5*s* and 6*s* orbital populations is close to 4 *e* thus demonstrating their small participation in the U-N chemical bonding. From the UPS and XPS investigations of the core and valence levels of UN, the popula-

Table 3. The Results of Current LCAO Calculations for UN Bulk.

Property		MT78	MT60	SC60
a_0 (4.89)		5.17	4.78	4.80
E_{tot}		−106.5218	−531.0228	−531.9898
E_U		−51.5970	−475.9572	−476.9186
E_c (13.6)		9.6	13.4	13.6
B (194)		167.2	291.6	276.9
Q_U		1.63	1.55	1.58
SD		3.18	1.18	1.06
Populations, *e*				
U	*s*	2.05	4.20	4.04
	p	5.98	12.03	12.15
	d	1.11	11.96	11.96
	f	3.23	2.26	2.27
N	*s*	3.89	3.87	3.87
	p	4.72	4.58	4.64
	d	0.02	0.10	0.07

The energy *per* unit cell E_{tot} and the U atom energy E_U (given in a.u.), the cohesive energy E_c (eV), the lattice constant a_0 (Å), and the bulk modulus *B* (GPa). The experimental values are given in brackets in the first column. The U atom spin density (SD) is given in μ_B.

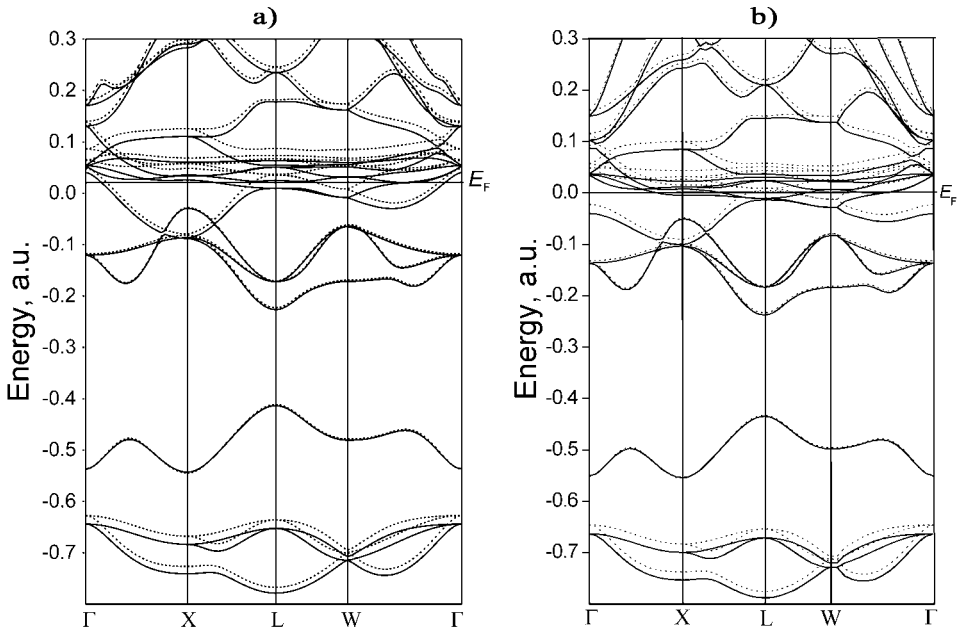

Figure 1. The energy bands of UN crystal constructed for: (a) LCAO PW91 (RECP 60) and (b) PW PW91 (RECP 78) Hamiltonians. The energies are given in a.u., solid and dotted lines correspond to the states with spin up and spin down, respectively.

tion of 2.2 ± 0.5 *e* in the U5*f* band near the Fermi level has been estimated.[17] This result is in good agreement with our DFT-LCAO (2.27 *e*, see Table 3) and FP LAPW (2.17 *e* [6]) values for U5*f* populations. As to U6*d* orbitals, their participation in the chemical bonding is seen from Table 3: for the RECP MT78, 6*d* population is 1.11 *e*, but for both RECPs-60 it is 1.96 *e*. It is also seen that the covalent part of bonding is defined mainly by N2*p* orbitals.

As follows from Table 3, the SD value in the ground state of metallic UN crystals is close to unity in the calculations with the RECP 60. The calculated spin-density of 1.06 μ_B (SC60) is the most close to the experimental value of 0.75 μ_B.[1] This result differs from that found in article[11,13] for different RECP 78 when the ground state with the spin projection 3/2 appeared to be more favorable (the three U5*f* electrons with parallel spins occupying the t_{2u} states near the Fermi level).

Figure 1a shows the upper part of the valence and the lower part of the conduction energy bands obtained in the LCAO DFT-PW91 calculations with the RECP SC60 for the total spin projection $S_z = 1/2$. The lowest in energy threefold degenerates subband and next nondegenerate subband are formed by U6*p* and U6*s*+N2*s* states, respectively. The next threefold subband centered at −0.10 a.u is formed by the hybridized U5*f* + N2*p* states. The highest subbands up to the Fermi level are formed mainly by U5*f* states. The more detailed analysis of the crystalline orbitals at the BZ shows, in particular, that the nondegenerate a_{2u} level is occupied by two (spin-up and spin-down) 5*f* electrons; the third 5*f* unpaired spin-up electron occupies three-fold degenerate t_{2g} level formed by U6*d* states. The relative position of different U5*f* subbands near the Fermi level depends on the RECP chosen. As it follows from ref. [13], the RECP78 calculations change the order of bands in such a way that three spin-up electrons occupy the states of three-fold band near the Fermi level. Thus, the spin density calculated depends on the RECP chosen (∼3 *e* for RECP78 and ∼1 *e* for the RECP60, see Table 3). The choice of the RECP SC60 is preferable, as it gives the best agreement with the experimentally known UN properties. Therefore, in our LCAO surface calculations to be analyzed in next section we used the RECP SC60 for the core electrons.

Computational procedure of the VASP code[25] used for our current DFT-PW calculations applies a standard iterative solution of the Kohn-Sham equations based on residuum-minimization and optimized charge-density mixing routines.[31] They include the calculations of the Hellmann-Feynman forces acting on the atoms and the stresses on the unit cell.[32] The total energy is optimized with respect to the positions of the atoms within the unit cell or supercell. For UN bulk PW calculations, we have applied the same 16 × 16 × 16 *k*-point mesh in the BZ in the framework of Monkhorst-Pack scheme[29] as used in LCAO calculations described above. The cut-off energy was chosen to be 520 eV for the PW91 and PBE Hamiltonians compared here. Main results of these calculations are presented in Table 4 and Figure 1b.

The conclusion could be drawn from the Table 4 that the two DFT functionals used give similar results close to the previous VASP calculations[10,11] performed with a smaller *k*-point mesh and the cut-off energy. A comparison of Tables 3 and 4 demonstrates a qualitative correlation of properties calculated using the LCAO (RECP 60) and the PW (RECP 78) methods, except for bulk modulus which is noticeably overestimated in the CRYSTAL calculations as compared with the experimental value.

The analysis of band structures for UN bulk presented in Figure 1 calculated by LCAO and PW methods using the same

Table 4. The Results of Current PW Calculations for UN Bulk and Their Comparison with Previously Published Data.

Property	PW91	PBE	PW91-PAW[10]	PBE-AE-LAPW[5,6]
a_0 (4.886)	4.868	4.867	4.864	4.886
E_c (13.6)	14.79	14.57	14.7	13.4
B (194)	227	224	226	209
Q_U	1.69	1.69	1.61	–
SD	1.15	1.19	1.05	1.25

See Table 3 footnote for explanation.

PW91 Hamiltonian demonstrates even good quantitative correlation in details especially below the Fermi level, in agreement with the experiment[7] and the previous DOS analysis performed in earlier PW VASP calculations.[11]

DFT LCAO and PW Calculations on UN(001) Surface

Single (2D) and Repeated (3D) Slab Models of a Surface

The single (2D) and repeated (3D) slab models are used in LCAO and PW surface calculations, respectively.[15] The LCAO calculations do not require artificial repeating of slab along the normal to the surface direction as it is made in PW calculations to restore 3D periodicity. However, use of atom-centered Gaussian BS faces in LCAO calculations a rather serious problem known as the basis-set superposition error (BSSE). The problem is that in a system comprising interacting fragments A and B, the fact that the basis sets on A and B are practically always incomplete means that the fragment energy of A has necessarily to be improved by the basis functions on B, irrespective there is any genuine binding interaction in the AB system or not. The improvement in the fragment energies lowers the energy of the combined AB system. The BSSE is an ever-present phenomenon and accurate calculations should always include the BSSE analysis. The examples when one should be particularly concerned include the binding energy of molecules adsorbed on surfaces or calculation of defect formation energies.[15] The approach most commonly used to estimate the BSSE effect is the *counterpoise correction*[33]: the separated fragment energies are computed not in the individual fragment basis sets, but the total basis set for the system including "ghost basis functions" for the fragment that is not present. These energies are then used to define the counterpoise-corrected (CPC) interaction energy.

In the bulk crystal the AO basis of a given atom is extended by AOs centered on atoms in the neighboring unit cells. However, in the slab calculations this is not true for surface atoms. This may lead to underestimate of the slab energy and as a consequence, to overestimate of the surface energy. Moreover, the AO used in the crystal and slab calculation may not be sufficiently diffused to reproduce correctly the electronic density distribution tail in the vacuum outside the surface. Corresponding corrections are similar to those arising for bulk solids and molecules. The simple and physically reasonable way to introduce the CPC interaction for the slab model of a surface (bare, reduced, relaxed) was suggested in ref. [34] and includes the addition of one and two extra layers of ghost atoms on both slab surfaces. The fixed ghost atoms are placed at their bulk positions, thus forming the crystallographic planes next to the surface atomic planes. The additional Gaussians are centered on the ghost atoms and called the extra layer basis set (ELBS). This approach was applied in ref. 34 in a study of water adsorption on $SrTiO_3$ (001) surface. The geometric structure of slabs was reoptimized, fixing the positions of the ghost atoms. It was found that addition of the first ELBS introduces noticeable changes in the calculated properties, whereas the second ELBS has no further effect. In particular, the BSSE correction reduces the surface energy of cubic semiconducting perovskites and decreases the water adsorption energy. For metallic UN crystal the large electron delocalization may increase the influence of the BSSE on the calculated surface energies and surface relaxation. This is demonstrated in the following section.

For DFT-PW surface calculations, we use 3D symmetric slabs consisting of 3–11 atomic layers separated by vacuum gaps up to 15 empty layers (see Fig. 2). This inter-slab distance is large enough to exclude interaction between the neighboring 2D slabs and to allow one the comparison of 2D LCAO and 3D PW results.

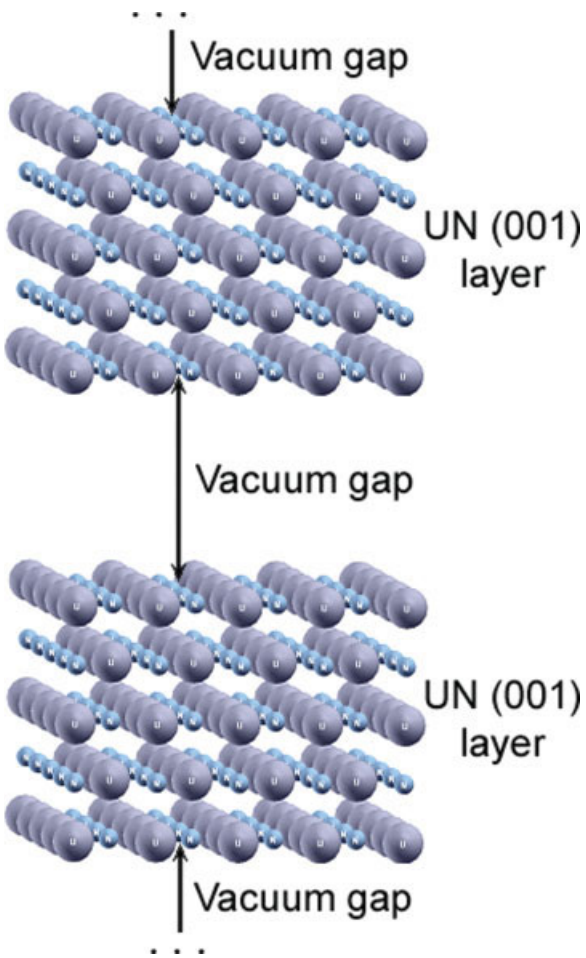

Figure 2. Side view of five-layer 3D slab model of the UN(001) surface.

Table 5. The Calculated Atomic Displacements Δz (Å) on UN (001) obtained for Different Slabs and Methods.

Atom	Method	Number of atomic planes in slab				
		3	5	7	9	11
Surface U	LCAO	−0.085	−0.095	–	–	–
	LCAO (extra layer added)	−0.026	−0.046	–	–	–
	PW PW91	−0.041	−0.020	−0.050	−0.061	−0.057
Subsurface U	LCAO		−0.011	–	–	–
	LCAO (extra layer added)		−0.001	–	–	–
	PW PW91		−0.018	−0.016	−0.013	−0.013
Surface N	LCAO	0.064	0.058	–	–	–
	LCAO (extra layer added)	0.049	0.048	–	–	–
	PW PW91	0.030	0.022	0.025	0.033	0.026
Subsurface N	LCAO		−0.002	–	–	–
	LCAO (extra layer added)		0.027	–	–	–
	PW PW91		0.026	0.028	0.032	0.022

Positive sign means an outward displacement from the slab center and *vice versa*.

In the PW surface calculations, we have used the PW91 Hamiltonian only, since a comparison between results of the PW91 and PBE calculations on UN bulk (Table 4) do not show any noticeable differences. We have applied the same Monkhorst-Pack scheme for the 8 × 8×1 *k*-point mesh. The cut-off energy was chosen 520 eV, similar to the bulk. All calculations were performed for the spin-polarized (FM) surface states.

Comparison of LCAO and PW Results for Unrelaxed and Relaxed Surface

We have analyzed in detail the vertical displacements along the *z* axis of both surface and subsurface atoms from their host lattice sites in UN bulk (Table 5), effective atomic charges (Table 6), the surface energies (Table 7) as well as DOS obtained in the PW calculations (see Fig. 3). The surface energy of an *n*-layer slab was estimated from the standard basic relationship:

$$E_{surf}(n) = \frac{1}{2S}(E_n - nE_b) \quad (2)$$

where E_n is the total slab energy per primitive surface unit cell and S its area, while E_b is the total energy per primitive bulk unit cell.

There is a good qualitative agreement between structural relaxations and effective atomic charges for the LCAO with the

Table 6. The Effective Atomic Charges $q(e)$ on the UN (001) Slab.

Atom	Method	Number of atomic planes in slab				
		3	5	7	9	11
Surface U	LCAO	1.63	1.63	–	–	–
	LCAO (extra layer added)	1.64	1.64	–	–	–
	PW PW91	1.65	1.66	1.72	1.67	1.65
Subsurface U	LCAO	–	1.51	–	–	–
	LCAO (extra layer added)	–	1.55	–	–	–
	PW PW91	–	1.65	1.63	1.63	1.69
Middle U (mirror plane of slab)	LCAO	1.45	1.57	–	–	–
	LCAO (extra layer added)	1.52	1.55	–	–	–
	PW PW91	1.62	1.67	1.72	1.65	1.62
Surface N	LCAO	−1.55	−1.55	–	–	–
	LCAO (extra layer added)	−1.61	−1.60	–	–	–
	PW PW91	−1.64	−1.63	−1.64	−1.63	−1.67
Subsurface N	LCAO	–	−1.59	–	–	–
	LCAO (extra layer added)	–	−1.57	–	–	–
	PW PW91	–	−1.67	−1.7	−1.64	−1.7
Middle N (mirror plane of slab)	LCAO	−1.61	−1.58	–	–	–
	LCAO (extra layer added)	−1.58	−1.57	–	–	–
	PW PW91	−1.65	−1.7	−1.66	−1.62	−1.64

Table 7. Surface Energies E_{surf} (J m^{-2}) and Relaxation Energies E_{rel} (eV) obtained for UN(001) Surface in LCAO and Plane Wave Calculations.

Number of atomic planes in slab			3	5	7	9	11
Method	LCAO	E_{surf} (unrelaxed)	2.20	2.29	2.28	2.11	–
		E_{surf} (relaxed)	2.06	2.13	–	–	–
		E_{rel}	0.203	0.230	–	–	–
	LCAO (extra layer added)	E_{surf} (unrelaxed)	1.68	1.45	–	–	–
		E_{surf} (relaxed)	1.430	1.38	–	–	–
		E_{rel}	0.359	0.121	–	–	–
	Plane waves PW91	E_{surf} (unrelaxed)	1.81	1.87	1.84	1.86	1.90
		E_{surf} (relaxed)	1.70	1.69	1.70	1.70	1.69
		E_{rel}	0.156	0.258	0.210	0.239	0.305

extra-layer and the corresponding PW data (Table 5). First of all, in both methods atomic displacements have the same directions: N atoms go outwards from the surface whereas U atoms relax inwards, to the slab center. This is a pattern typical for the rumpling observed on oxide surfaces but the rumpling in UN is considerably larger. One observes also substantially larger magnitudes of surface U displacements than N atoms, whereas subsurface atom relaxations are smaller.

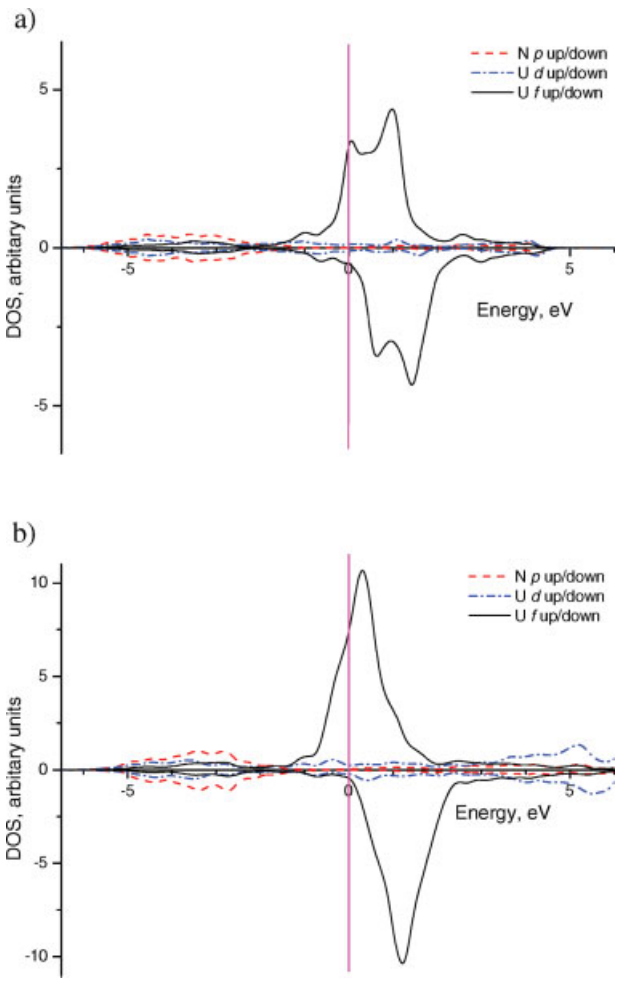

Figure 3. The projected DOS for the bulk (a) and the perfect UN(001) surface (b) in FM states.

There is also a good agreement of the effective atomic charges calculated in the LCAO and PW using two very different methods (Table 6). These charges indicate a considerable U-N bond covalency in both UN bulk and on the surface. Asymmetrical electron charge redistribution on U and N atoms is likely caused by atomic displacements from a crystalline 2D plane.

The surface energies are stabilized for slab thicknesses around 5–7 layers whereas the relaxation energy is more sensitive to the thickness (Table 7). Because of lack of experimental results, the calculated values of surface energy could be qualitatively compared only with 1.0–1.2 J/m^2 obtained recently for UO_2(001) surface energy using the quantum mechanical calculations.[2] As one can see, the surface energies of UN(001) and UO_2(001) are predicted to be similar. A qualitative agreement is observed between the UN(001) surface energies obtained in the LCAO calculations using extra-layer and the PW calculations. Increase of the number of atomic layers in the UN(001) slab stabilizes the energy of relaxed surface.

The total and projected DOS in the FM state obtained in our PW calculations is present in Figure 3. There is a small difference in band shapes from previous UN bulk calculation,[11] due to the much higher *k*-point mesh and cut-off energy used here. A comparison of the bulk DOS (Fig. 3a) with that for the projection of the surface U and N atoms (Fig. 3b) shows mainly changes in the shape of unoccupied states above the Fermi level. In both cases the mixed metallic-covalent chemical occurs with U5*f* states at the Fermi level, which is in line with previous experimental and theoretical studies[1,4–6,8].

Conclusions

In this article, we demonstrated an importance of choice of the proper effective core potentials in actinide (U) compound calculations which can considerably change the results obtained (e.g., the magnetic structure). We have also shown that the reliable LCAO calculations of the surface properties needs introduction

of an extra layer of the ghost functions simulating correct electronic density decay into vacuum from the surface. All this allowed us to perform first detailed study on properties of the densely packed UN(001) surface.

The results obtained by means of two substantially different DFT methods—LCAO and PW—demonstrate good agreement. We observed considerable relaxation of surface atoms which affects the surface energy. These results will be used in further study of surface defects and processes, first of all, UN surface oxidation which is important practical problem for its use as advanced nuclear fuel.

Acknowledgments

Authors are indebted to A. V. Titov, N. S. Mosyagin, P. Weck, A. Ray, D. Sedmidubsky, E. Heifets, Yu. Mastrikov, D. Gryaznov, and P. van Uffelen for fruitful discussions (DG, YM also for a technical assistance). D. B. gratefully acknowledges funding from the European Social Fund (ESF). This study was partly supported by the EC Framework 7 EURATOM.

References

1. Matzke, H. Science of Advanced LMFBR Fuels; North Holland: Amsterdam, 1986.
2. Skomurski, F. N.; Ewing, R. C.; Rohl, A. L.; Gale, J. D.; Becker, U. Am Mineral 2006, 91, 1761.
3. Weinberger, P.; Mallett, C. P.; Podloucky, R.; Neckel, A. J Phys C: Solid State Phys 1980, 13, 173.
4. (a) Brooks, M. S.; Glotzer, D. Phys B 1980, 102, 51; (b) Brooks, M. S. J Phys F: Met Phys 1984, 14, 639.
5. Sedmidubsky, D.; Konings, R. J. M.; Novak, P. J Nucl Mat 2005, 344, 40.
6. Atta-Fynn, R.; Ray, A. K. Phys Rev B 2007, 76, 115101.
7. Ito, T.; Kumigashira, H.; Souma, S.; Tahakashi, T.; Suzuki, T. J Magn Magn Mater 2001, 68, 226.
8. (a) Black, L.; Miserque, F.; Gouder, T.; Havela, L.; Rebizant, J.; Wastin, F. J Alloys Compd 2001, 315, 36; (b) Rafaja, D.; Havela, L.; Kuzel, R.; Wastin, F.; Colineau, E.; Gouder, T. J Alloys Compd 2005, 386, 87.
9. Yongbin, Z.; Daqiao, M.; Zhenghe, Z.; Meizhong, M. Chin J Chem Phys 2005, 18, 735.
10. Kotomin, E. A.; Mastrikov, Yu.; Zhukovskii, Yu. F.; Van Ufflen, P.; Rondinella, V. V. Phys Status Solidi C 2007, 4, 1193.
11. Kotomin, E. A.; Grimes, R. W.; Mastrikov, Yu.; Ashley, N. J. J Phys: Condens Matter 2007, 19, 106208.
12. Weck, P. F.; Kim, E.; Balakrishnan, N.; Poineau, F.; Yeamans, C. B.; Czerwinski, K. R. Chem Phys Lett 2007, 443, 82.
13. Evarestov, R. A.; Losev, M. V.; Panin, A. I.; Mosyagin, N. S.; Titov, A. V. Phys Status Solidi C 2008, 245, 114.
14. Perdew, J. P.; Wang, Y. Phys Rev B 1992, 45, 13244.
15. Evarestov, R. A. Quantum Chemistry of Solids. The LCAO First Principles Treatment of Crystals, Springer Series in Solid State Sciences, Vol. 153; Springer: Berlin, 2007.
16. Kudin, K. N.; Scuseria, G. E.; Martin, R. L. Phys Rev Lett 2002, 89, 266402.
17. Marutzky, M.; Barkow, U.; Schoenes, J.; Troc, R. J Magn Magn Mater 2006, 299, 225.
18. De Jong, W. A.; Harrison, R. J.; Nichols, J. A.; Dixon, D. A. Theor Chem Acc 2001, 107, 22.
19. Batista, E. R.; Martin, R. L.; Hay, P. J.; Peralta, J. E.; Scuseria, G. E. J Chem Phys 2004, 121, 2144.
20. Kuchle, W.; Dolg, M.; Stoll, H.; Preuss, H. J Chem Phys 1994, 100, 7535.
21. Titov, A. V.; Mosyagin, N. S. Int J Quantum Chem 1999, 71, 359.
22. Mosyagin, N. S.; Petrov, A. N.; Titov, A. V.; Tupitsyn, I. I. Progr Theor Chem Phys B 2006, 15, 229.
23. Bunday, B. D. Basic Optimization Methods; Edward Arnold: London, 1984.
24. Press, W. H.; Teukolski, S. A.; Vetterling, V. T.; Flannery, B. P. Numerical Recipes in Fortran 77: The Art of Scientific Computing; Cambridge University Press: Cambridge, 1997.
25. Kresse, G.; Hafner, J. VASP the Guide, University of Vienna, 2007. Available at: http://cms.mpi.univie.ac.at/vasp.
26. Blöchl, P. E. Phys Rev B 1994, 50, 17953.
27. Frisch, M. J.; Trucks, G. W.; Schlegel, H. B.; Scuseria, G. E.; Robb, M. A.; Cheeseman, J. R.; Montgomery, Jr., J. A.; Vreven, T.; Kudin, K. N.; Burant, J. C.; Millam, J. M.; Iyengar, S. S.; Tomasi, J.; Barone, V.; Mennucci, B.; Cossi, M.; Scalmani, G.; Rega, N.; Petersson, G. A.; Nakatsuji, H.; Hada, M.; Ehara, M.; Toyota, K.; Fukuda, R.; Hasegawa, J.; Ishida, M.; Nakajima, T.; Honda, Y.; Kitao, O.; Nakai, H.; Klene, M.; Li, X.; Knox, J. E.; Hratchian, H. P.; Cross, J. B.; Bakken, V.; Adamo, C.; Jaramillo, J.; Gomperts, R.; Stratmann, R. E.; Yazyev, O.; Austin, A. J.; Cammi, R.; Pomelli, C.; Ochterski, J. W.; Ayala, P. Y.; Morokuma, K.; Voth, G. A.; Salvador, P.; Dannenberg, J. J.; Zakrzewski, V. G.; Dapprich, S.; Daniels, A. D.; Strain, M. C.; Farkas, O.; Malick, D. K.; Rabuck, A. D.; Raghavachari, K.; Foresman, J. B.; Ortiz, J. V.; Cui, Q.; Baboul, A. G.; Clifford, S.; Cioslowski, J.; Stefanov, B. B.; Liu, G.; Liashenko, A.; Piskorz, P.; Komaromi, I.; Martin, R. L.; Fox, D. J.; Keith, T.; Al-Laham, M. A.; Peng, C. Y.; Nanayakkara, A.; Challacombe, M.; Gill, P. M. W.; Johnson, B.; Chen, W.; Wong, M. W.; Gonzalez, C.; and Pople, J. A. GAUSSIAN-03, Revision C. 02; Gaussian Inc.: Wallingford, CT, 2004. Available at: http://www.gaussian.com/.
28. Dovesi, R.; Saunders, V. R.; Roetti, C.; Orlando, R.; Zicovich-Wilson, C.M.; Pascale, F.; Civalleri, B.; Doll, K.; Harrison, N. M.; Bush, I.J.; D'Arco, Ph.; Llunell, M. CRYSTAL-06, Users Manual, University of Turin, 2006. Available at: http://www.crystal.unito.it.
29. Monkhorst, H. J.; Pack, J. D. Phys Rev B 1976, 13, 5188.
30. Available at: https://bse.pnl.gov/bse/portal.
31. (a) Kresse, G.; Furthmüller, J. J Comput Mater Sci 1996, 6, 15; (b) Kresse, G.; Furthmüller, J. Phys Rev B 1996, 54, 11169.
32. (a) Kresse, G.; Hafner, J. Phys Rev B 1993, 48, 13115; (b) Kresse, G.; Hafner, J. Phys Rev B 1994, 49, 14251.
33. Boys, S. F.; Bernardi, F. Mol Phys 1970, 19, 553.
34. Evarestov, R. A.; Bandura, A. V.; Alexandrov, V. E. Surf Sci 2007, 601, 1844.

Surface Science 603 (2009) 50–53

Contents lists available at ScienceDirect

Surface Science

journal homepage: www.elsevier.com/locate/susc

First principles calculations of oxygen adsorption on the UN(001) surface

Yu.F. Zhukovskii [a], D. Bocharov [a,*], E.A. Kotomin [b], R.A. Evarestov [c], A.V. Bandura [c]

[a] Institute for Solid State Physics, Kengaraga 8, LV–1063 Riga, Latvia
[b] European Commission, Joint Research Centre, Institute for Transuranium Elements, Hermann von Helmholtz Pl. 1, D-76344 Eggenstein-Leopoldshafen, Germany
[c] Department of Quantum Chemistry, St. Petersburg State University, Universitetsky Prosp. 26, 198504 St. Petergof, Russia

ARTICLE INFO

Article history:
Received 18 August 2008
Accepted for publication 13 October 2008
Available online 22 October 2008

Keywords:
Density functional calculations
Uranium nitride
Chemisorption
Oxygen

ABSTRACT

Fabrication, handling and disposal of nuclear fuel materials require comprehensive knowledge of their surface morphology and reactivity. Due to unavoidable contact with air components (even at low partial pressures), UN samples contain considerable amount of oxygen impurities affecting fuel properties. In this study we focus on reactivity of the energetically most stable (001) substrate of uranium nitride towards the atomic oxygen as one of initial stages for further UN oxidation. The basic properties of O atoms adsorbed on the UN(001) surface are simulated here combining the two first principles calculation methods based on the plane wave basis set and that of the localized orbitals.

The actinide nitrides and carbides, *e.g.,* uranium mononitride (UN) with a face centered cubic (fcc) rock salt structure, belong to the family of non-oxide ceramic nuclear fuels considered as promising candidates for the use in Generation-IV fast nuclear reactors. These materials reveal several advantages over traditional UO_2 fuel (*e.g.*, higher thermal conductivity and metal density) [1]. One of the problems with nitride and carbide fuels is their active interaction with the oxygen which results in an effective fuel oxidation and degradation [2]. This could affect the fabrication process as well as the fuel performance and safety. First experimental studies on O in UN were performed in 80ies ([1] and references therein). These activities were continued recently combining several techniques ([2] and references therein). However, understanding of the atomistic mechanism of fuel oxidation needs first principles theoretical modeling. Thus, to shed more light on this problem, we study here theoretically the interaction of atomic oxygen with the UN(001) surface.

Theoretical simulations of uranium compounds are especially complicated due to a relativistic character of an electron motion in the U atomic core and the strong electron–electron correlation. Moreover, UN is characterized by a mixed metal-covalent chemical bonding. Physical and chemical properties of light actinides are determined by partly localized *5f* electrons, which determine a number of properties, such as mixed valence, magnetism, etc. A series of first principles DFT calculations on pure and defective UO_2 were performed recently (*e.g.*, [3–8]) whereas a number of similar calculations on the nitride fuels is still much more limited [9–15]. In our recent paper [15] the methodology was proposed for LCAO calculations of the UN surface properties. The first results on the pure UN surfaces were presented therein using two approaches based on the basis sets of atomic orbitals (AO) and plane waves (PW), respectively. Use of the two different methods greatly increases the reliability of the results obtained.

To simplify modeling of the oxygen interaction with UN powder surface, we study here only the (001) surface which according to Tasker [16] has the lowest energy. To simulate the perfect UN(001) substrate as well as its interaction with oxygen, we have employed the DFT-PW computer code *VASP 4.6* [17] based on the use of a plane wave basis set and the method of projector–augmented–waves (PAW) for atomic core description. We apply the non-local exchange-correlation functional Perdew-Wang-91 using the generalized gradient approximation (GGA) [18] and the scalar relativistic PAW pseudopotentials representing the U core electrons (with $6s^2 6p^6 6d^2 5f^2 7s^2$ valence shell), N ($2s^2 2p^3$) and O ($2s^2 2p^4$) atoms (containing 14, 5 and 6 valence electrons, respectively). The cut-off energy has been chosen to be 520 eV. We use the Monkhorst–Pack scheme [19] with mainly $8 \times 8 \times 1$ *k*-point meshes in the Brillouin zone (BZ).

As the second method, we have used the *CRYSTAL-06* computer code [20] based on the Gaussian-type functions centered on the atomic nuclei as the basis sets for expansion of the linear combination of atomic orbitals (LCAO). We use the non-local exchange-correlation functional PBE [21]. The oxygen basis set (BS) 8-411G(1*d*) was taken from Ref. [22]. For the N atom, the all-electron BS 6-311G(2*d*) has been used [23]. Finally, for the U atom we have used the energy-adjusted relativistic small core (60 electrons in core) effective potential from Ref. [24]. To get rid of the basis set linear

* Corresponding author. Tel.: +371 67187480; fax: +371 67132778.
E-mail address: bocharov@latnet.lv (D. Bocharov).

0039-6028/$ - see front matter © 2008 Elsevier B.V. All rights reserved.
doi:10.1016/j.susc.2008.10.019

dependence in the *CRYSTAL* LCAO calculations, the diffuse *s*-, *p*-, *d*- and *f*- Gaussian-type orbitals with exponents < 0.2 a.u.$^{-1}$ have been removed from the basis sets. The exponents of other polarization functions have been reoptimized, to restore the required precision in the total energy. High accuracy in both *k*-set mesh and DFT integration grid (XLGRID) has been applied for all *CRYSTAL-06* calculations. Prior to a study of surface properties, the bulk structure optimization of UN crystal has been performed using the LCAO approach. The Monkhorst–Pack scheme [19] with $16 \times 16 \times 16$ *k*-point mesh for the BZ sampling and $32 \times 32 \times 32$ *k*-point Gilat [25] net for the calculation of the Fermi energy and density matrix have been used here.

When modeling the UN(001) surface, we have used symmetric slabs consisting of five atomic layers with regularly alternating uranium and nitrogen atoms [15]. Plane wave computational formalism requires the use of an artificial slab translation in a vertical direction with a period called the *vacuum gap*. The magnitude of the latter (38.8 Å for five-layer UN slab), was found large enough to exclude the interaction between the repeated slabs for all single slab models studied using the PAW approach The slabs in the LCAO calculations have been really two-dimensional. The optimized lattice constant (4.87 for PAW *VASP vs.* 4.81 Å for LCAO *CRYSTAL* calculations) has been used in all further calculations, with an error within 2% of the experimental value (4.89 Å) [1]. Only ferromagnetic UN ground state has been considered in this study as the energetically most preferable state at low temperatures. The calculations of UN bulk structure suggest the magnetic moment on the U cation ~1 μ_B. Thus, for five-layers slab the total magnetic moment of a 2×2 2D supercell (containing 20 U cations and 20 N anions) in both approaches has been fixed at 20 μ_B.

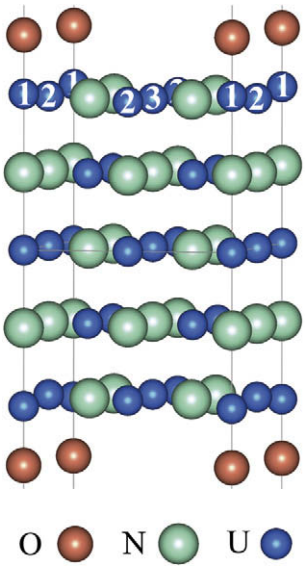

Fig. 1. A model of two-sided periodic adsorption of O atoms (0.25 ML) atop the surface U cations. Numbers enumerate non-equivalent interfacial atoms.

To simulate the O atom adsorption, we have used the same supercell model with a periodic adsorbate distribution. These supercells with the 2×2 extension of surface translation vectors correspond to the atomic O coverage of 0.25 ML. To reduce computational efforts, we have considered symmetric two-sided arrangement of oxygen adatoms (Fig. 1). We have simulated two configurations of atomic adsorption: O atop the surface U cation or N anion (Fig. 1) with the complete structural optimization. For PAW calculations on the O/UN(001) interface using 3D slab model, we should also check whether the vacuum gap of 38.8 Å for a five-layer slab of uranium nitride [15] is large enough for the models additionally containing adsorbed O atoms from both sides.

The binding energy E_{bind} of adsorbed oxygen O_{ads} was calculated with respect to a free O atom

$$E_{bind} = \frac{1}{2}\left(E_{tot}^{UN} + 2E_{tot}^{O_{triplet}} - E_{tot}^{O/UN}\right), \quad (1)$$

where $E_{tot}^{O/UN}$ is the total energy of a fully relaxed O/UN(001) slab for O_{ads} positions atop either the N or U surface ions, $E_{tot}^{O_{triplet}}$ and E_{tot}^{UN} the energies of an isolated O atom in the ground (triplet) state and of a pure relaxed slab. In PAW calculations of free O atom, the cubic box with the same periodicity as for the O/UN(001) and UN(001) 3D slabs has been used. The factor 1/2 before brackets appears since the substrate is modeled by slab with the two equivalent surfaces and O_{ads} is positioned symmetrically with respect to the surfaces.

Due to a mixed metallic-covalent nature of the chemical bonding in UN [10–14], we expect a high affinity of O_{ads} towards the UN(001) substrate. The binding energy *per* O adatom is expected to be closer to that on a regular O/Al(111) and (001) metallic interfaces (~10 eV) [26] than on semiconducting O/$SrTiO_3$(001) interfaces (with two possible SrO- or TiO_2-terminations) (~2eV) [27]. Indeed, we have obtained in the *VASP* calculations the binding energies of 6.9 and 5.0 eV *per* O adatom atop the surface U or N ions, respectively, accompanied with 0.9–1.2 *e* charge transfer from the surface towards the O adatom (Tables 1 and 2). The positively charged surface U cation goes outwards, to the adsorbed O atom whereas in the O configuration atop the N anion the latter is

Table 1
The calculated binding energy (E_{bind}), the distance between O and surface U cation (d_{O-U}), the effective atomic charges (q), and vertical (Δz) U and N displacements from the surface plane for adatom position atop the surface U (Fig. 1). The effective charges of U and N ions on the pure surface are equal to +1.63 *e* for surface U cation and −1.55 *e* for surface N anion in LCAO 5-layer slab calculations as well as +1.66 *e* for surface U cation and −1.63 *e* for surface N anion in PAW 5-layer slab calculations [15].

Method of calculation	E_{bind}, eV	q(O), *e*	q(U1), *e*	q(U2), *e*	q(U3), *e*	q(N), *e*	d_{O-U}, Å	Δz(U1), Å	Δz(U2), Å	Δz(U3), Å	Δz(N), Å
LCAO[a]	8.3	−0.89	1.97	1.66	1.62	−1.56	1.87	+0.15[b]	−0.07	−0.11	−0.04
PAW[c]	6.9	−1.04	1.96	1.86	1.83	−1.60	1.91	+0.135[b]	−0.02	−0.04	−0.05

[a] LCAO–PBE calculations performed with *CRYSTAL-2006* code.
[b] Positive sign corresponds to atom displacement outward from the substrate.
[c] PAW–PW91 calculations performed with *VASP-4.6* code.

Table 2
The calculated parameters for O atom adsorption atop the surface N anion[a]. See caption and footnotes of Table 1 for explanation.

Method of calculation	E_{bind}, eV	q(O), *e*	q(N1), *e*	q(N2), *e*	q(N3), *e*	q(U), *e*	d_{O-N}, Å	Δz(N1), Å	Δz(N2), Å	Δz(N3), Å	Δz(U), Å
PAW	5.0	−1.20	−1.44	−1.56	−1.59	−1.56	2.19	−0.64	+0.065	+0.06	+0.10

[a] Atomic positions of U and N ions are reversed as compared to those shown in Fig. 1.

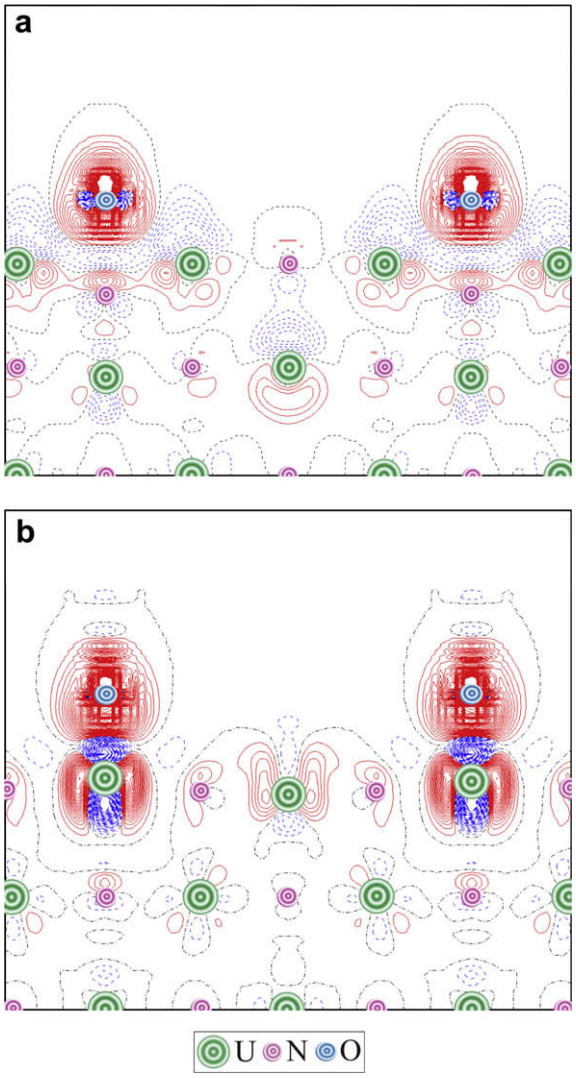

Fig. 2. The difference electron density maps $\Delta\rho$ (**r**) (the total density of the interface minus the densities of substrate and adsorbate with optimized interfacial geometry) for the O adatoms atop the surface: (a) N anions and (b) U cations on the UN(001) surface obtained using results of PAW calculations. Solid (red) and dashed (blue) isolines correspond to positive and negative electron density, respectively. Isodensity increment is 0.003 e Å^{-3}. (For interpretation of the references to color in this figure legend, the reader is referred to the web version of this article).

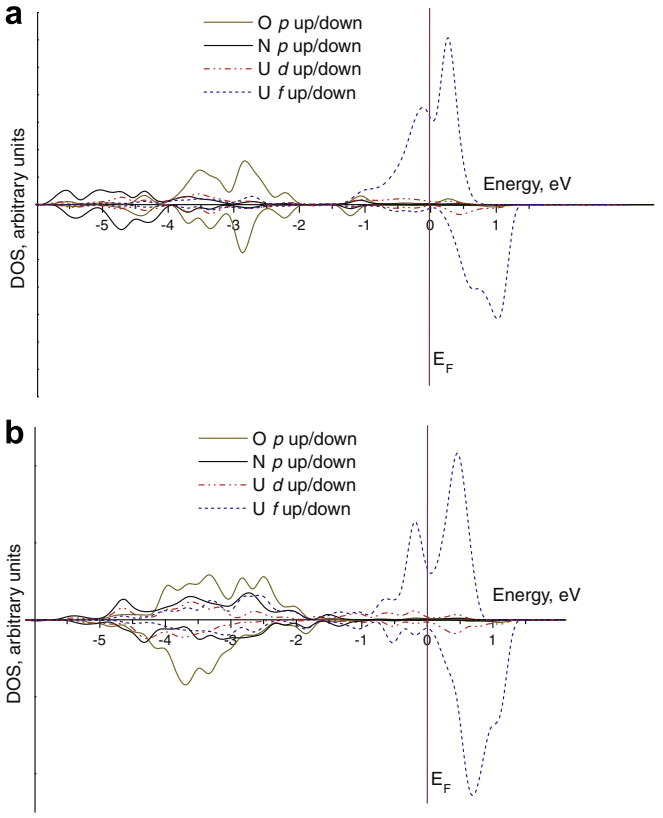

Fig. 3. The total and projected densities of states for O adsorption atop the N anion (a) and the U cation (b) obtained using results of PAW calculations. In the former, we consider the orbital projections of N anion under O atom and one of four nearest neighbouring U cations (Fig. 2a). Analogously, the lower plot presents the orbital projections of U cation beneath adatom and one of four nearest N anions. The largest peaks have been normalized to the same value, whereas a convolution of individual energy levels has been plotted using the Gaussian functions with a half-width 0.2 eV. "O" on energy axis corresponds to Fermi level.

strongly displaced from the adsorbed O atom towards the slab center, due to a mutual repulsion.

The corresponding results of *VASP* and *CRYSTAL* calculations based on the two very different methods demonstrate a good qualitative agreement for O adatom properties atop the surface U ion (Table 1) in all properties: the binding energies (3D slab models usually underestimate this parameter due to a weak repulsion between the adjacent polarized slabs), atomic displacements and even effective charges (which are calculated using the very different Mulliken (LCAO) and Bader (PAW) procedures).

An analysis of the difference electron charge redistributions for both configurations of O_{ads} (Fig. 2) confirms that the O adatom forms a strong chemical bonding with the surface U cation which could be considered as one-site complex. In the case of O adatom atop the surface N anion this is rather multi-center adsorption complex involving four adjacent surface U ions. As follows from Table 1, these cations mostly contribute to the high O binding energy atop the N anion.

Adsorption of O_{ads} atop the surface N or U ions on the UN(001) surface leads to appearance of the specific oxygen bands in the density of states (DOS) (Fig. 3) as compared to DOS for a pure UN(001) surface [15]. For oxygen atop the surface U cation, O *2p* states overlap with the U *6d* and with a well-pronounced tail of U *5f* states in the region of the N *2p* valence band (−2 to −4 eV). This indicates once more a strong oxygen chemical bonding (chemisorption) on U, typical for metal surfaces. However, when O is located atop N, the U *5f* contribution in this energy region diminishes whereas N *2p* states are considerably pushed down to smaller energies, due to N anion repulsion from negatively charged O adatom.

Summing up, the results obtained here for oxygen interaction with UN surfaces demonstrate strong chemisorption typical for metallic surfaces and could serve as the first important step in understanding the initial stage of the oxidation mechanism. The excellent agreement of the results obtained using two very different first principles methods supports their reliability. We continue the study of O_2 dissociation and the diffusion path of O_{ads} on both perfect and defective UN(001) substrates, which is aimed at understanding atomistic mechanism of oxidation by means of substitution of surface N ions for O ions.

Acknowledgements

The authors kindly thank P. Van Uffelen, R. Caciuffo, D. Gryaznov, V. Kashcheyevs, A. Kuzmin, M. Losev, Yu. Mastrikov, S. Piskunov for fruitful discussions and for valuable help with the calculations. This study was partly supported by the Service Contract 205343-2006-07 F1ED KAR LV between ITU, Karlsruhe, and

ISSP, Riga, EC Framework 7 Project F-Bridge, and the proposal N25592 from EMS Laboratory of the PNNL. D. Bocharov gratefully acknowledges support from the European Social Fund (ESF).

References

[1] Hj. Matzke, Science of Advanced LMFBR Fuel, North Holland, Amsterdam, 1986;
P.D. Wilson (Ed.), The Nuclear Fuel Cycle, University Press, Oxford, 1996.
[2] H. Wiame, M. Centeno, S. Pacard, P. Bastian, P. Grange, J. Eur. Ceram. Soc. 18 (1998) 1293;
M. Walter, Oxidation of Inert Matrices, JRC-ITU-TN-2005/35.
[3] T. Petit, C. Lemaignan, F. Jollet, B. Bigot, A. Pasturel, Philos. Mag. B 77 (1998) 779.
[4] J.P. Crocombette, F. Jollet, L. Thien Nga, T. Petit, Phys. Rev. B 64 (2001) 104107.
[5] K. Kudin, G. Scuseria, R. Martin, Phys. Rev. Lett. 89 (2002) 266402.
[6] L. Petit, A. Svane, S. Szotek, W.M. Temmerman, Science 301 (2003) 498.
[7] M. Freyss, T. Petit, J.P. Crocombette, J. Nucl. Mater. 347 (2005) 44.
[8] H.Y. Geng, Y. Chen, Y. Kaneta, M. Kinoshita, Phys. Rev. B 75 (2007) 054111.
[9] M.S.S. Brooks, D. Glötzel, Physica B 102 (1980) 51;
M.S.S. Brooks, J. Phys. F: Met. Phys. 14 (1984) 639.
[10] D. Sedmidubsky, R.J.M. Konings, P. Novak, J. Nucl. Mater. 344 (2005) 40.
[11] E.A. Kotomin, Yu.A. Mastrikov, Yu.F. Zhukovskii, P. Van Uffelen, V.V. Rondinella, Phys. Status Solidi C 4 (2007) 1193.
[12] E.A. Kotomin, R.W. Grimes, Yu.A. Mastrikov, N.J. Ashley, J. Phys.: Cond. Matt. 19 (2007) 106208.
[13] M. Samsel-Czekała, E. Talik, P. de V. Du Plessis, R. Troć, H. Misiorek, C. Sułkowski, Phys. Rev. B 76 (2007) 144426.
[14] R.A. Evarestov, M.V. Losev, A.I. Panin, N.S. Mosyagin, A.V. Titov, Phys. Status Solidi B 245 (2008) 114.
[15] R.A. Evarestov, A.V. Bandura, M.V. Losev, E.A. Kotomin, Yu.F. Zhukovskii, D. Bocharov, J. Comput. Chem. 29 (2008) 2079.
[16] P.W. Tasker, J. Phys. C Solid. State 12 (1979) 4977.
[17] G. Kresse, J. Hafner, VASP the Guide, University of Vienna, 2007, <http://cms.mpi.univie.ac.at/vasp/>.
[18] J.P. Perdew, Y. Wang, Phys. Rev. B 45 (1992) 13244.
[19] H.J. Monkhorst, J.D. Pack, Phys. Rev. B 13 (1976) 5188.
[20] R. Dovesi, V.R. Saunders, C. Roetti, R. Orlando, C.M. Zicovich-Wilson, F. Pascale, B. Civalleri, K. Doll, N.M. Harrison, I.J. Bush, Ph. D'Arco, M. Llunell, CRYSTAL2006 User's Manual, Universita di Torino, Torino, 2006, <http://www.crystal.unito.it/>.
[21] J.P. Perdew, K. Burke, M. Ernzerhof, Phys. Rev. Lett. 77 (1996) 3865.
[22] S. Piskunov, E. Heifets, R.I. Eglitis, G. Borstel, Comput. Mater. Sci. 29 (2004) 165.
[23] M.J. Frisch, J.A. Pople, J.S. Binkley, J. Chem. Phys. 80 (1984) 3265.
[24] W. Kuchle, M. Dolg, H. Stoll, H. Preuss, J. Chem. Phys. 100 (1994) 7535.
[25] G. Gilat, Phys. Rev. B 26 (1982) 2243.
[26] Yu.F. Zhukovskii, P.W.M. Jacobs, M. Causà, J. Phys. Chem. Solids 64 (2003) 1317.
[27] S. Piskunov, Yu.F. Zhukovskii, E.A. Kotomin, E. Heifets, D.E. Ellis, MRS Proc. 894 (2006) LL08-05.

Journal of Nuclear Materials 393 (2009) 504–507

Contents lists available at ScienceDirect

Journal of Nuclear Materials

journal homepage: www.elsevier.com/locate/jnucmat

Chemisorption of a molecular oxygen on the UN(0 0 1) surface: *Ab initio* calculations

Yu.F. Zhukovskii, D. Bocharov *, E.A. Kotomin

Institute of Solid State Physics, University of Latvia, 8 Kengaraga Street, LV-1063 Riga, Latvia

ARTICLE INFO

Article history:
Received 18 November 2008
Accepted 21 July 2009

ABSTRACT

The results of DFT GGA calculations on oxygen molecules adsorbed upon the (0 0 1) surface of uranium mononitride (UN) are presented and discussed. We demonstrate that O_2 molecules oriented parallel to the substrate can dissociate either (i) spontaneously when the molecular center lies above the surface hollow site or atop N ion, (ii) with the activation barrier when a molecule sits atop the surface U ion. This explains fast UN oxidation in air.

1. Introduction

The uranium mononitride (UN), which possesses a rock salt structure and metallic nature, is an advanced material for the non-oxide nuclear fuel considered as a promising candidate for the use in Generation-IV fast nuclear reactors. UN reveals several advantages over a traditional UO_2-type fuel (*e.g.*, higher thermal conductivity and metal density). However, one of important problems with actinide nitrides is their effective oxidation in contact with oxygen which can affect nuclear fuel performance [1].

There was a series of *ab initio* density functional theory (DFT) calculations published in last 10 years on pure and defective UO_2 (*e.g.*, [2–10]). Similar calculations on the UN appeared only recently [11–16]. In our recent papers, we studied both the structure of a perfect UN(0 0 1) surface [17] and chemisorption of oxygen atoms upon it [18]. These DFT calculations were performed using the two quite different computer codes: *VASP 4.6* [19], with plane wave basis set (BS), and *CRYSTAL-06* [20], with the BS of localized atomic orbitals (LCAO approach). In both cases we have applied the non-local exchange-correlation functional by Perdew–Wang-91 (PW91), that is, the generalized gradient approximation (GGA) [21]. The results of these two different methods reveal good agreement [17,18] which supports their reliability. A strong *chemisorption* was observed for a single O atom interaction with the UN surface (~7 eV is the binding energy atop the surface U ion) [18] which is typical for traditional metallic surfaces (*cf.* ~ 10 eV *per* adatom bound on the close-packed Al surfaces [22]). However, to shed more light on the UN oxidation mechanism, we study theoretically in this paper the interaction of *molecular* oxygen with the same defectless UN(0 0 1) surface. The key questions are: whether the O_2 dissociation upon the surface is energetically possible, which adsorption sites are optimal for this, and whether it can occur spontaneously, without energy barrier. These are important issues for understanding the mechanism of the oxidation of uranium nitride in air.

2. Theoretical

We have employed the *VASP 4.6* code [19] with the relativistic PAW pseudopotentials representing the core electrons of U ($6s^2 6p^6 6d^2 5f^2 7s^2$ valence shell), N ($2s^2 2p^3$) and O ($2s^2 2p^4$) atoms as well as the non-local PW91 exchange correlation functional [21]. The cut-off energy has been chosen 520 eV. We have applied the Monkhorst–Pack scheme [23] with $4 \times 4 \times 1$ k-point mesh in the Brillouin zone (BZ). When modeling the UN(0 0 1) surface, we have used the same 3D symmetric slabs as previously [17,18] consisting of five non-polar layers, containing alternating U and N atoms, separated by large vacuum gaps along the z-axis (~36 Å) and thus excluding the direct interaction of oxygen molecules from the neighboring slabs. The lattice constant (4.87 Å) optimized for the bulk has been used in all our slab calculations accompanied by a full structure optimization. The DFT GGA calculations suggest *ferromagnetic* ground state [24] of UN which contradicts the experimental observations of AFM phase at low temperatures [1]. Our test calculations [17] have confirmed that the FM phase is energetically more favorable also for the UN slab.

For simulation of the chemisorption of oxygen molecule, we have used mainly the 2×2 extended surface supercell (containing 20 U cations and 20 N anions), similarly to the previous study on chemisorption of an atomic oxygen [18]. The periodic adsorbate distribution corresponds to the molecular coverage of 0.25 ML (or atomic O coverage of 0.5 ML). To reduce computational efforts, we have used a symmetric two-sided arrangement of oxygen molecules on both surfaces of the slab. The energy gain E_{gain} *per* oxygen atom in the adsorbed molecule $(O_2)_{ads}$ arising after approach of the O_2 molecule towards the UN surface has been calculated as

$$E_{gain} = \frac{1}{4}\left(E^{UN} + 2E^{O_2} - E^{O_2/UN}\right), \quad (1)$$

* Corresponding author. Tel.: +371 67187480; fax: +371 67132778.
E-mail address: bocharov@latnet.lv (D. Bocharov).

0022-3115/$ - see front matter © 2009 Elsevier B.V. All rights reserved.
doi:10.1016/j.jnucmat.2009.07.010

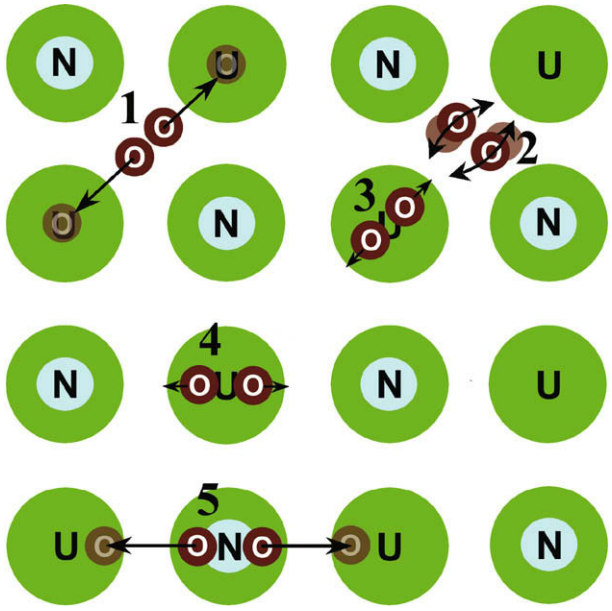

Fig. 1. Schematic view of five different horizontal configurations for the O_2 molecule adsorption on UN surface: (1) atop the hollow site oriented towards the nearest surface U ions, (2) atop the hollow site oriented towards the nearest surface N ions, (3) atop the surface U ions oriented towards the next-nearest surface U ions, (4) atop the surface U ions oriented towards the nearest surface N ions, (5) atop the surface N ions oriented towards the nearest surface U ions. We show, using arrows, that molecule spontaneous dissociation can occur when O_2 is located either atop the hollow site (1) or atop ion N (5).

where $E^{O_2/UN}$ is the total energy of a fully relaxed O_2/UN(0 0 1) slab for several configurations of $(O_2)_{ads}$ upon the substrate (with a center of molecule atop the corresponding surface site as shown in Fig. 1), E_2^O and E^{UN} the total energies of an isolated oxygen molecule in the ground (triplet) state and of a pure relaxed slab, respectively. The factor 1/4 before brackets appears since the substrate is modeled by a slab containing the two equivalent surfaces with $(O_2)_{ads}$ positioned symmetrically relatively to both slab surfaces whereas each molecule before and after dissociation contains two oxygen atoms. Similar analysis was earlier performed by us for various O_2/Al interfaces [22].

To compare the binding energy (E_{bind}) for the atomic oxygen adsorption atop the surface uranium atom calculated by us earlier [18] with the E_{gain} *per* dissociated oxygen adatom (Table 1), one should add about half the binding energy of oxygen molecule to the latter energy. The calculated E_{bind} for a free O_2 molecule in the triplet state is 6.06 eV and a bond length of 1.31 Å (*cf.* with the experimental values of 5.12 eV and 1.21 Å [25], respectively).

3. Main results

When modeling the molecular adsorption, we have analyzed different configurations of an O_2 molecule in the triplet state on the UN(0 0 1) substrate. *Vertical* orientations of the molecule atop the surface N or U ions have been found metastable with respect to molecule reorientation to the *horizontal* configuration, parallel to the surface. We have estimated both the energy gain of molecular adsorption using Eq. (1) and the O_2 dissociation energy (for some configurations), *i.e.*, the difference of the total energies of a slab with an oxygen molecule before and after dissociation, when the two O atoms in the triplet state which sit atop the two nearest surface U ions (Table 1).

3.1. Spontaneous dissociation of O_2 molecules

We have found that a spontaneous, barrierless O_2 dissociation indeed takes place in the two cases: when the molecular center is atop either (i) a hollow site or (ii) surface N ion, with the molecular bond directed towards the two nearest surface U ions (the configurations 1 and 5 in Fig. 1, respectively). The relevant dissociation energies E_{diss} are given in Table 1, along with other parameters characterizing the atomic relaxation and the Bader charge distribution. To estimate energy gain for intermediate molecular adsorption in these two configurations (as present in Table 1) we have fixed the O_2 bond length as in a gas phase allowing the molecule to relax only along a distance from the surface. Geometry and charges for the configurations 1 and 5 after dissociation (Table 1) are in general similar to those obtained in our previous study [18] for UN(0 0 1) substrate covered by chemisorbed O atoms, *e.g.*, surface U atoms beneath the oxygen adatom after dissociation are shifted up in both configurations. An increase of the surface supercell size from 2×2 up to 3×3 results in the 10% growth of the E_{gain} due to a reduced repulsion between the periodically distributed adatoms (Table 1).

We have also identified two other configurations of adsorbed oxygen molecules where the dissociation is energetically possible but with the energy barrier: (i) atop the hollow site when a molecular bond is oriented towards the nearest N ions (the configuration 2 in Fig. 1) and (ii) atop the surface U ion (for any molecular orientation, *e.g.*, the configurations 3 and 4 in Fig. 1). For the configuration 2, we have observed the orientation instability of the adsorbed molecule which easily rotates, *e.g.*, towards the surface U ion with further dissociation. The configurations 3 and 4 could be characterized as rather metastable UO_2 quasi-molecules due to a strong bonding between all three atoms (Fig. 2c) and since the corresponding U ion is noticeably shifted up from its initial positions on surface (Table 1). Meanwhile, the dissociation of $(O_2)_{ads}$ molecule in the configuration 3 is energetically possible but only after overcoming the small (~0.3 eV) activation energy barrier.

Table 1
The calculated energy gains (E_{gain}, Eq. (1)) and dissociation E_{diss} energies (eV), geometry (z, Δz) and charges (q) for configurations of molecular and spontaneous dissociative chemisorption of oxygen molecule above the UN(0 0 1) substrate. Numbers in brackets correspond to the configurations shown in Fig. 1.

Position		E_{gain} *per* O atom, eV	z[a], Å	E_{diss}, eV	q(O), *e*	q(U1[b]), *e*	q(U2[c]), *e*	q(N[d]), *e*	Δz[e](U1), Å	Δz[e](U2), Å	Δz[e](N), Å
Hollow (1)	Molecular adsorption	1.185	1.893	–	−0.465	1.913	1.762	−1.533	−0.0496	−0.0496	0.02498
	After dissociation	4.21	1.957	3.025	−0.978	2.053	1.978	−1.577	0.075	0.068	−0.133
Atop U	Towards next-nearest U (3)	2.15	2.18	–	−0.5905	2.042	1.836	−1.6065	0.176	−0.048	−0.096
	Towards nearest N (4)	2.33	2.14	–	−0.578	2.0485	1.827	−1.6248	0.123	−0.051	−0.106
Atop N (5)	Molecular adsorption	0.82	2.020	–	−0.5685	1.8675	1.8322	−1.3537	−0.0496	−0.0496	0.025
	After dissociation	4.00[f]	1.955	3.18	−0.979	2.115	1.876	−1.580	0.073	0.021	−0.201

[a] z is the height of O atoms respectively the non-relaxed UN substrate.
[b] U1 the nearest surface U ion.
[c] U2 the next-nearest surface U ion.
[d] N the nearest surface N ion.
[e] Δz the additional vertical shifts of the same surface ions from their positions in the absence of adsorbed oxygen.
[f] 4.40 eV for 3×3 extended surface supercell.

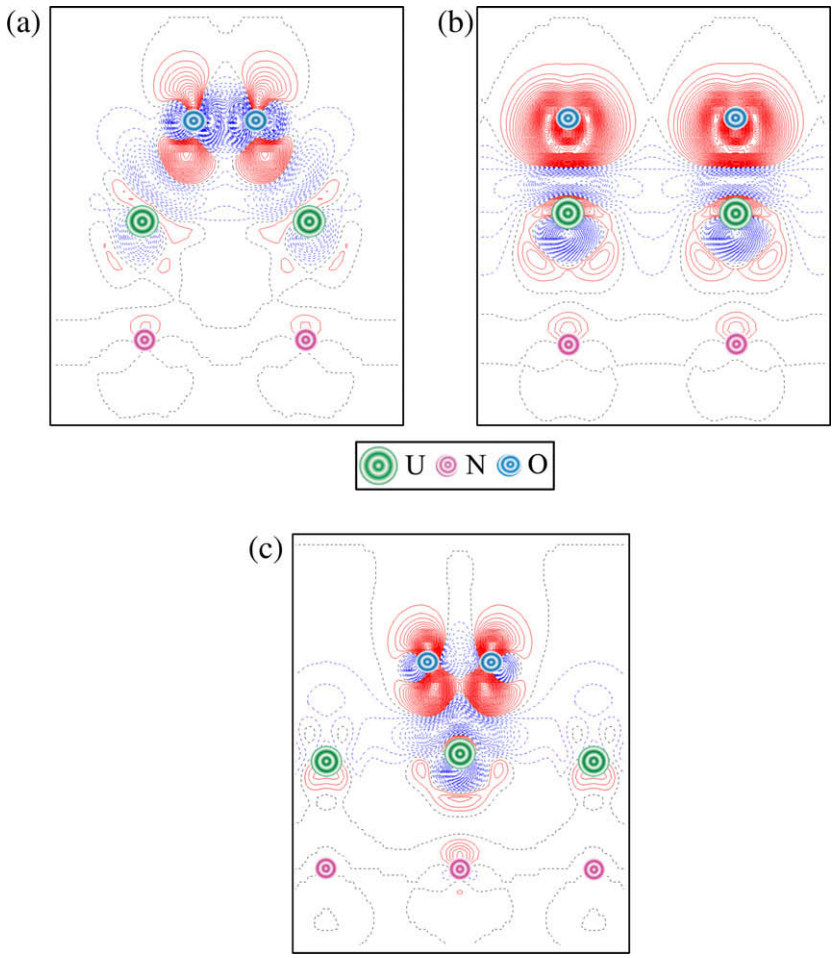

Fig. 2. The difference electron density maps $\Delta\rho$ (r) (the total density of the interface minus the sum of densities of substrate and adsorbate with optimized interfacial geometry) for (a) the O_2 molecule upon the hollow position oriented to the nearest surface U ions, (b) after its dissociation in the configuration 1 (Fig. 1) with O atoms atop the surface U ions and (c) for the O_2 molecule atop the surface U ion in the configuration 3 (Fig. 1). Solid (red) and dashed (blue) isolines correspond to positive (excess) and negative (deficiency) electron density, respectively. Isodensity increment is 0.003 e Å^{-3}. (For interpretation of the references to colour in this figure legend, the reader is referred to the web version of this article.)

3.2. Charge redistribution analysis

Adsorption of an O_2 molecule (in the triplet state) is accompanied by the charge transfer of $\sim$1 e (*per* molecule) from the substrate (Table 1). In Fig. 2 we analyze the difference electron charge redistributions for three configurations of horizontally oriented $(O_2)_{ads}$ upon the surface: (a) molecule adsorbed upon the hollow site (the configuration 1, Fig. 1), (b) molecule dissociated from this configuration with O adatoms located atop the nearest surface U ions, and (c) molecule adsorbed upon the surface U ion (the configuration 3). Spontaneous O_2 dissociation and thus a smooth transition from the charge distribution (a) to (b) can be explained by continuous areas of the electron density (Fig. 2a) parallel to the surface which may be considered as *dissociation channels*, analogously to the density plot for a molecular oxygen upon the Al substrate [22]. After dissociation each O adatom contains an extra charge of $\sim$1 e, *i.e.*, transforms into O^- ion in the triplet state (Fig. 2b). In contrast, when considering the molecular configuration 3, these *dissociation channels* are transformed into *dissociation barriers* (Fig. 2c). Simultaneously, we observe considerably higher electron density, indicating a kind of UO_2 quasi-molecule with a strong bonding between the O_2 molecule and surface U atom beneath. Thus, difference between the electron density plots presented in Fig. 2a and c can explain different dissociation abilities of O_2 molecule in the configurations 1 and 3 (Fig. 1).

3.3. Electronic densities of states (DOS)

For the same adsorbate configurations considered above, we have constructed the total and projected densities of states (DOS) (Fig. 3). Molecular adsorption in these configurations leads to appearance of the specific *oxygen bands* as compared to those for oxygen adatoms upon UN surface [18] and O atom substituted for a host N ion in UN bulk [15]. For a molecular oxygen atop the hollow position (Fig. 3a), O 2*p* peak is observed at -1 eV overlapping with the U 5*f* and 6*d* bands. After O_2 dissociation (Fig. 3b) this peak disappears being replaced by the broad two-peak band in the region of the N 2*p* valence band (-2 to -5 eV), similarly to the DOS for oxygen adatoms on UN(0 0 1) substrate [18]. Some differences are also noticeable between the corresponding U 5*f* and 6*d* peaks in the spectral range above -1 eV (*cf.* Fig. 3a and b) which could be caused by both different arrangement of O and U atoms in these configurations and sensitivity of uranium states to the presence of oxygen, thus indicating once more a strong oxygen chemical bonding (chemisorption). When oxygen molecule is located atop the surface U ion (the configuration 3), the U 5*f* and 6*d* contributions in the energy range above -1 eV are diminished, simultaneously the O 2*p* contribution grows, thus increasing an overlap between all three states and indicating UO_2 quasi-molecular bond formation. As compared to the adsorption of oxygen molecule upon the hollow site (Fig. 3a), we again observe a higher O 2*p* peak

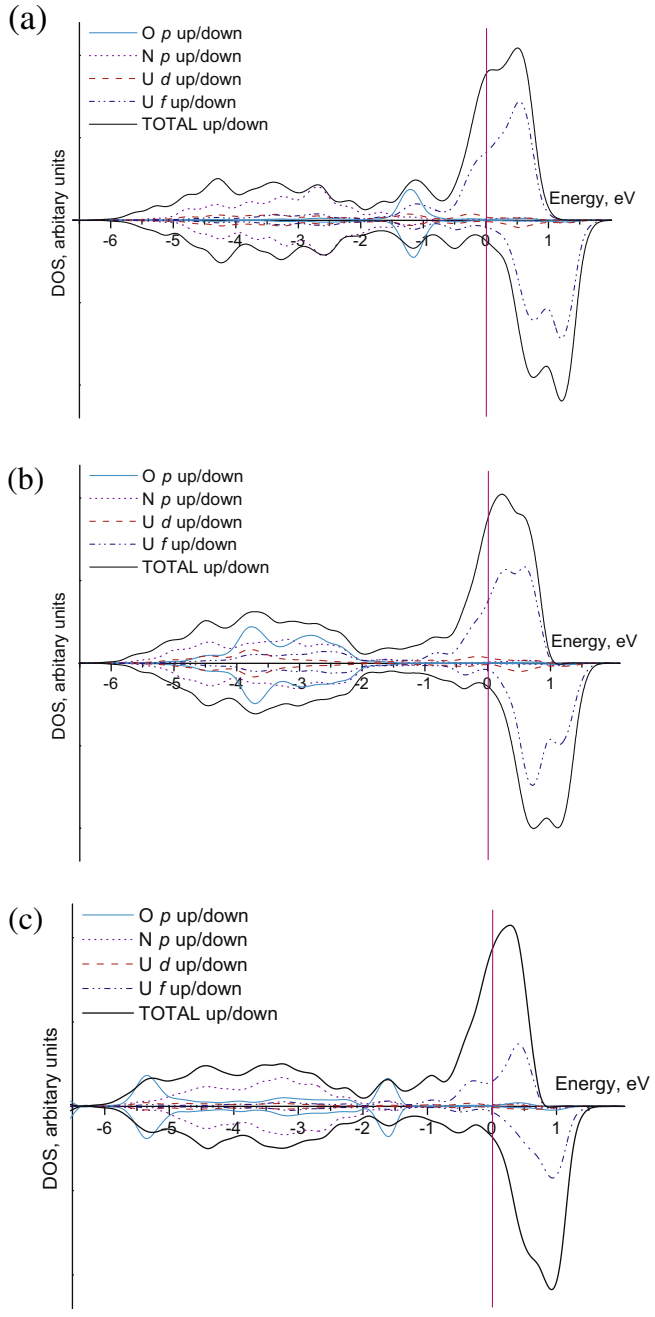

Fig. 3. The total and projected densities of states for three configurations of O_2 molecule as in Fig. 2 (the same a, b and c). The orbital projections of both O atoms as well as the nearest N and U ions are shown. The highest peaks have been normalized to the same value, whereas a convolution of individual energy levels has been plotted using the Gaussian functions with a half-width of 0.2 eV.

(at −1.5 eV) and an additional lower peak of the same O 2*p* (at −5.5 eV) which noticeably overlaps with the U 5*f* and 6*d* subpeaks (Fig. 3c). Similarity with the latter pattern was observed earlier for the projected DOS of O atom substituted for N in UN bulk [15]. In all three DOS (Fig. 3), a broad band corresponding to the N 2*p* projected states does not change drastically which means a weak effect of N ions on the O_2 molecule adsorption on the UN(0 0 1) surface.

4. Conclusions

Summing up, the results of our *ab initio* calculations clearly demonstrate a real possibility for spontaneous dissociation of the adsorbed oxygen molecules upon the perfect UN(0 0 1) surface, analogously to the O_2 dissociation on "traditional" metallic surfaces. This is the important step in understanding the initial stage of the UN oxidation mechanism.

Acknowledgements

This study was partly supported by the European Community FP7 project F-Bridge. D.B. gratefully acknowledges also the support from the European Social Fund (ESF). The authors kindly thank R. Caciuffo, R.A. Evarestov, D. Gryaznov, E. Heifets, Yu. Mastrikov, Hj. Matzke, and P. Van Uffelen for fruitful discussions.

References

[1] (a) Hj. Matzke, Science of Advanced LMFBR Fuel, North Holland, Amsterdam, 1986;
(b) Hj. Matzke, in: P.D. Wilson (Ed.), The Nuclear Fuel Cycle, University Press, Oxford, 1996.
[2] T. Petit, C. Lemaignan, F. Jollet, B. Bigot, A. Pasturel, Philos. Mag. B 77 (1998) 779.
[3] J.P. Crocombette, F. Jollet, L. Thien Nga, T. Petit, Phys. Rev. B 64 (2001) 104107.
[4] K. Kudin, G. Scuseria, R. Martin, Phys. Rev. Lett. 89 (2002) 266402.
[5] L. Petit, A. Svane, S. Szotek, W.M. Temmerman, Science 301 (2003) 498.
[6] M. Freyss, T. Petit, J.P. Crocombette, J. Nucl. Mater. 347 (2005) 44.
[7] F.N. Skomurski, R.C. Ewing, A.L. Rohl, J.D. Gale, U. Becker, Amer. Mineralog. 91 (2006) 1761.
[8] F. Gupta, G. Brillant, A. Pasturel, Philos. Mag. 87 (2007) 2561.
[9] (a) H.Y. Geng, Y. Chen, Y. Kaneta, M. Kinoshita, Phys. Rev. B 75 (2007) 054111; (b) H.Y. Geng, Y. Chen, Y. Kaneta, M. Kinoshita, Phys. Rev. B 77 (2008) 104120.
[10] P. Nerikar, T. Watanabe, J.S. Tulenko, S.R. Phillpot, S.B. Sinnott, J. Nucl. Mater. 384 (2009) 61.
[11] D. Sedmidubsky, R.J.M. Konings, P. Novak, J. Nucl. Mater. 344 (2005) 40.
[12] E.A. Kotomin, Yu.A. Mastrikov, Yu.F. Zhukovskii, P. Van Uffelen, V.V. Rondinella, Phys. Status Solidi (c) 4 (2007) 1193.
[13] E.A. Kotomin, R.W. Grimes, Yu.A. Mastrikov, N.J. Ashley, J. Phys.: Condens. Matter 19 (2007) 106208.
[14] M. Samsel-Czekała, E. Talik, P.V. Du Plessis, R. Troć, H. Misiorek, C. Sułkowski, Phys. Rev. B 76 (2007) 144426.
[15] E.A. Kotomin, Yu.A. Mastrikov, J. Nucl. Mater. 377 (2008) 492.
[16] R.A. Evarestov, M.V. Losev, A.I. Panin, N.S. Mosyagin, A.V. Titov, Phys. Status Solidi (b) 245 (2008) 114.
[17] R.A. Evarestov, A.V. Bandura, M.V. Losev, E.A. Kotomin, Yu.F. Zhukovskii, D. Bocharov, J. Comput. Chem. 29 (2008) 2079.
[18] Yu.F. Zhukovskii, D. Bocharov, E.A. Kotomin, R.A. Evarestov, A.V. Bandura, Surf. Sci. 603 (2009) 50.
[19] G. Kresse, J. Hafner, VASP the Guide, University of Vienna, 2007, <http://cms.mpi.univie.ac.at/vasp/>.
[20] R. Dovesi, V.R. Saunders, C. Roetti, R. Orlando, C.M. Zicovich-Wilson, F. Pascale, B. Civalleri, K. Doll, N.M. Harrison, I.J. Bush, Ph. D'Arco, M. Llunell, CRYSTAL2006 User's Manual, Universita di Torino, Torino, 2006, <http://www.crystal.unito.it/>.
[21] J.P. Perdew, Y. Wang, Phys. Rev. B 45 (1992) 13244.
[22] Yu.F. Zhukovskii, P.W.M. Jacobs, M. Causá, J. Phys. Chem. Solids 64 (2003) 1317.
[23] H.J. Monkhorst, J.D. Pack, Phys. Rev. B 13 (1976) 5188.
[24] R. Atta-Fynn, A.K. Ray, Phys. Rev. B 76 (2007) 115101.
[25] R. Weast, CRC Handbook of Chemistry and Physics, CRC Press Inc., Boca Baton, FL, 1985.

Surface Science 605 (2011) 396–400

Contents lists available at ScienceDirect

Surface Science

journal homepage: www.elsevier.com/ locate/susc

DFT calculations of point defects on UN(001) surface

D. Bocharov [a,b,c,*], D. Gryaznov [a], Yu.F. Zhukovskii [a], E.A. Kotomin [a]

[a] Institute for Solid State Physics, Kengaraga 8, LV-1063 Riga, Latvia
[b] Faculty of Physics and Mathematics, University of Latvia, Zellu 8, LV-1002 Riga, Latvia
[c] Faculty of Computing, University of Latvia, Raina blvd 19, LV-1586 Riga, Latvia

ARTICLE INFO

Article history:
Received 31 August 2010
Accepted 15 November 2010
Available online 27 November 2010

Keywords:
Density functional theory calculations
Uranium mononitride
(001) surface
Surface defects

ABSTRACT

The density functional theory is used in a study of point defects on both UN(001) surface and sub-surface layers. We compare the results for slabs of different thicknesses (both perfect and containing nitrogen or uranium vacancies) with a full geometry, electronic and spin density optimization. The electronic charge density re-distribution, density of states, magnetic moments of U atoms and local atomic displacements around defects are carefully analyzed. It is predicted that the vacancies are formed easier on the surface, whereas the property of sub-surface layer does not differ significantly from the central one in the slab.

1. Introduction

Uranium mononitride (UN) is considered nowadays by the Generation IV International Forum of nuclear reactors [1] as one of the promising nuclear fuels alternative to UO_2. However, it reveals unwanted oxidation in air [2] which could affect the fuel fabrication process and its performance. Atomistic understanding of the oxidation process could help to solve this problem.

Previous first-principles simulations on UN used mostly the density functional theory (DFT) and were focused mainly on bulk properties (for example, [3–9]). To check reliability of these results, we performed recently several calculations on bulk and (001) surface of UN using the two different DFT approaches [10]: linear combination of atomic orbitals (LCAO) applied for construction of basis sets and plane waves (PW) combined with the pseudopotentials representing the core electrons, as implemented in both *CRYSTAL* [11] and *VASP* [12] computer codes. Our basic findings for the bulk and the (001) surface of UN calculated using the *VASP* code were confirmed by *CRYSTAL* calculations [10]. The results of both series of calculations on the lattice constant, bulk modulus, cohesive energy, charge distribution, band structure and density of states (DOS) for UN single crystal were analyzed.

Recently [13,14], we performed first-principles simulations on the atomic and molecular oxygen interaction with the perfect UN(001) surface. It was demonstrated that the O_2 molecules could spontaneously dissociate [14] at the defect-free surface and releasing O adatoms reveal strong chemical interaction with surface ions [13]. It is worth mentioning that all our UN surface calculations [10,13,14] were performed for the fixed magnetic moments of U atoms.

To understand the oxidation mechanism in more detail, one has to take into account surface defects and their interaction with oxygen. So far, only point defects in the UN bulk were calculated [15,16]. In this paper, we study basic properties of surface vacancies. In section 2, a slab model and parameters used in our present spin-polarized PW DFT calculations are described. In section 3, we discuss main results obtained for the N and U vacancies on the surface. A short summary is presented in section 4.

2. Slab model and computational details

UN possesses a rock-salt *fcc* structure over a wide temperature range. We model the (001) surface using the symmetrical slabs containing odd number (5, 7, 9 or 11) of atomic layers separated by the vacuum gap of 38.9 Å which corresponds to 16 inter-layers (Fig. 1). Atomic layers consist of regularly alternating N and U atoms. Our test calculations show that such an inter-slab distance is large enough to exclude spurious interactions between the slabs repeated in the *z*-direction.

To simulate single point defects (either N or U vacancies), we applied a supercell approach using unit cells with 2×2 and 3×3 extensions of surface translation vectors. These supercells contain four and nine pairs of atoms in each layer while periodically distributed surface vacancies for such unit cells correspond to defect concentrations of 0.25 and 0.11 monolayers (ML), respectively. We calculated not only the outer surface defects, but also the sub-surface defects as well as those positioned at the central layer of the slab. To reduce computational efforts, we considered the two-side arrangement of the point defects which is symmetrical with respect to the central (mirror) plane (the atomistic model of surface N vacancies with the 2×2 periodicity is shown in Fig. 2).

* Corresponding author. Institute for Solid State Physics, Kengaraga 8, LV-1063 Riga, Latvia. Fax: +371 67132778.
E-mail address: bocharov@latnet.lv (D. Bocharov).

0039-6028/$ – see front matter © 2010 Elsevier B.V. All rights reserved.
doi:10.1016/j.susc.2010.11.007

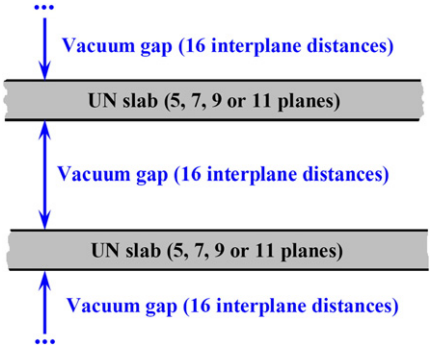

Fig. 1. Cross-section of UN(001) slabs.

For calculations, we used the PW DFT computer code *VASP 4.6* [12,17]. To represent the core electrons (78 electrons for U and 2 electrons for N), the relativistic pseudopotentials combined with the PAW method [18] were used. The Perdew-Wang-91 non-local exchange-correlation (GGA) functional [19] was chosen for calculations. The cut-off energy was fixed at 520 eV. The Monkhorst-Pack *k*-point mesh [20] of $8\times8\times1$ for integration over the Brillouin zone (BZ) was used, whereas the electron occupancies were determined following Methfessel and Paxton [21] as implemented in the *VASP* code. The smearing parameter of 0.2 eV was found to be optimal for reasonable convergences, suggesting the electronic entropy contribution of the order of 10 meV. The total energy of slabs of different thicknesses was optimized with respect to the atomic positions only, with the lattice parameter fixed at its equilibrium value of 4.87 Å for UN bulk. This value is slightly underestimated as compared to the experimental bulk value of 4.89 Å [22]. The ferromagnetic state was chosen for all our slab calculations [3] performed for the self-consistent (relaxed) atomic magnetic moments with no spin-orbit interactions included. Consequently, we calculated both the effective atomic charges and average magnetic moments per atom using the topological Bader analysis [23,24].

3. Main results

3.1. Perfect UN(001) surface

First, the calculations of the effective atomic charges q^{eff}, atomic displacements Δr, average magnetic moments μ_{av} of U atoms, and surface energies E_{surf} for defect-free slabs of different thicknesses

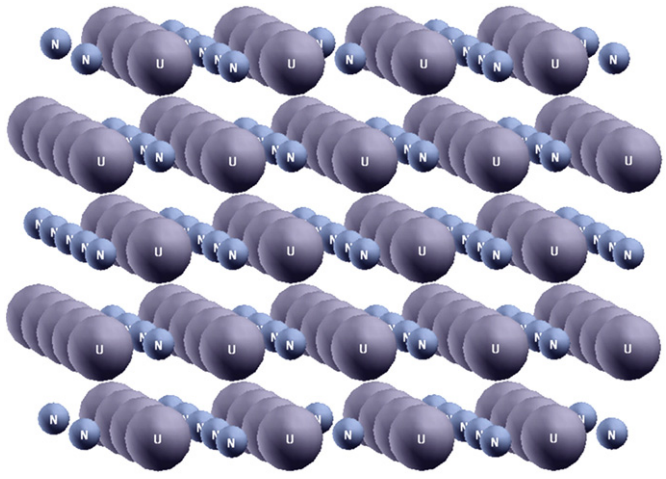

Fig. 2. Five-layer slab containing the two-sided surface N vacancies with a 2×2 periodicity.

Table 1
Surface energies E_{surf} ($\text{J}\cdot\text{m}^{-1}$) for calculations with relaxed and unrelaxed atomic spins as well as averaged magnetic moment (in μ_B) of U atom for the defect-free UN(001) surface.

Number of atomic planes	E_{surf} (spin-unrelaxed slab)	E_{surf} (spin-relaxed slab)	μ_{av}
5	1.69	1.44	1.57
7	1.70	1.37	1.44
9	1.70	1.29	1.37
11	1.69	1.22	1.33

(Tables 1 and 2) were performed, in order to check how these properties depend on atomic spin relaxation (in our previous calculations the total magnetic moment of a slab was fixed [10,13,14]). The spin relaxation leads to considerable change of E_{surf} depending on the number of layers in a slab (Table 1). The largest μ_{av} value was obtained for the U atoms in the 5-layer slab, i.e., μ_{av} slightly decreases with the thickness, suggesting difference of 0.3 μ_B between the 5- and 11-layer slabs. The lattice relaxation energies in spin-optimized calculations turn out to be quite small, i.e., ~0.03 eV.

It is also interesting to analyze q^{eff} values for atoms across the slab as a function of the number of layers in a slab (Table 2). First, q^{eff} shows considerable covalent bonding both on the surface (e.g., sub-surface) and on the central plane since the values are quite far from the formal ionic charges $\pm3e$. Second, the values in Table 2 demonstrate that the surface is slightly positively charged, due to a difference in the N and U charges. Third, the atomic charges are insensitive to both the spin relaxation and the number of layers.

The atomic displacements Δz from perfect lattice sites differ significantly for U atoms positioned at the surface and sub-surface layers (Table 3) being somewhat larger for the 5-layer slab while displacements of nitrogen atoms for all the slabs remain almost unchanged. Note that N atoms at (001) surface are displaced up, whereas U atoms are shifted inwards the slab center which results in the surface rumpling up to 1.2% of the lattice constant.

3.2. Vacancies on the (001) surface

In the present study, we considered the two reference states in calculations of the defect formation energies, both widely used in

Table 2
Atomic Bader charges on a defect-free surface.

Atom	Number of atomic layers			
	5	7	9	11
Surface U	1.68	1.74	1.68	1.72
Sub-surface U	1.67	1.63	1.63	1.67
U in central (mirror) plane	1.69	1.72	1.65	1.66
Surface N	−1.65	−1.67	−1.67	−1.68
Sub-surface N	−1.68	−1.70	−1.70	−1.67
N in central (mirror) plane	−1.74	−1.65	−1.65	−1.63

Table 3
Atomic displacements Δz(Å)* for defect-free surface (spin-relaxed calculations).

Number of atomic planes	U atom displacements		N atom displacements	
	Surface	Sub-surface	Surface	Sub-surface
5	−0.050	−0.012	0.023	0.023
7	−0.046	−0.009	0.024	0.028
9	−0.047	−0.011	0.024	0.028
11	−0.047	−0.011	0.025	0.031

*Negative sign means an inward atomic displacement towards the slab center.

Table 4
The vacancy formation energies (in eV) for the two reference states (see the text for details).

Layer	Number of atomic planes in slab and supercell extension (in brackets)	Reference I, Eqs. (1a)–(2)[a]		Reference II, Eqs. (1a), (1b), (3a) and (3b)[b]	
		U	N	U	N
Surface layer	5 (2×2)	8.63	8.84	1.46	3.70
	7 (2×2)	8.61	8.84	1.44	3.70
	9 (2×2)	8.61	8.84	1.44	3.71
	11 (2×2)	8.60	8.85	1.43	3.71
	5 (3×3)	8.51	8.78	1.34	3.64
	7 (3×3)	8.47	8.78	1.30	3.65
Sub-surface layer	5 (2×2)	10.31	9.38	3.14	4.25
	7 (2×2)	10.29	9.46	3.12	4.33
	9 (2×2)	10.26	9.46	3.09	4.33
	11 (2×2)	10.26	9.46	3.09	4.33
	7 (3×3)	10.18	9.47	3.01	4.34
Central (mirror) layer[c]	5 (2×2)	10.20	9.48	3.03	4.34
	7 (2×2)	10.36	9.57	3.19	4.43
	9 (2×2)	10.34	9.55	3.17	4.42
	11 (2×2)	10.39	9.56	3.22	4.42
	7 (3×3)	10.23	9.55	3.06	4.42

[a] Reference energies I equal to −4.10 eV for U atom and −3.17 eV for N atom.
[b] Reference energies II equal to −11.28 eV for U atom and −8.30 eV for N atom.
[c] Defect formation energies for UN bulk using reference I are 9.1–9.7 eV for N vacancy and 9.4–10.3 for U vacancy [15].

the literature. The point defect formation energy was calculated either as

$$E_{\text{form}}^{\text{N(U)vac}} = \frac{1}{2}\left(E_{\text{def}}^{\text{UN}} + 2E_{\text{ref\_I(II)}}^{\text{N(U)}} - E^{\text{UN}}\right), \tag{1a}$$

for surface and sub-surface vacancies, or

$$E_{\text{form}}^{\text{N(U)vac}} = E_{\text{def}}^{\text{UN}} + E_{\text{ref\_I(II)}}^{\text{N(U)}} - E^{\text{UN}}, \tag{1b}$$

for a vacancy in the central layer of the slab. Here $E_{\text{def}}^{\text{UN}}$ is the total energy of fully relaxed slab containing N (or U) vacancies, E^{UN} the same for a defect-free slab, while $E_{\text{ref\_I(II)}}^{\text{N(U)}}$ is reference energy for N (or U) atom. In our study, we used the two different reference states for both N and U atoms. Note that the pre-factor of ½ in Eq. (1a) arises due to a mirror arrangement of two N (U) vacancies on the surface and sub-surface layers (Fig. 2).

The first reference corresponds to N (U) isolated atom in triplet (quartet) spin states determined by $2p^3$ ($5f^3 6d^1$) valence electron configurations (hereafter reference I as in Table 4) calculated in a large tetragonal box ($28.28 \times 28.28 \times 22$ Å^3), i.e.:

$$E_{\text{ref\_I}}^{\text{N(U)}} = E_{\text{atom}}^{\text{N(U)}} \tag{2}$$

The second reference state (hereafter reference II as in Table 4) represents the chemical potential of N (U) atom which is in general a function of temperature and nitrogen partial pressure. By neglecting these effects, the N chemical potential can be treated as the energy of atom in the molecule N_2. Consequently, the chemical potential of U atom is given by the one-half total energy (per unit cell) of U single crystal in its low-temperature α-phase having the orthorhombic structure [25]. Thus, the corresponding second reference energies can be estimated as:

$$E_{\text{ref\_II}}^{\text{N}} = \mu_{N_2} = \frac{1}{2}E_{\text{tot}}[N_2], \tag{3a}$$

$$E_{\text{ref\_II}}^{\text{U}} = \mu_{\alpha-U} = \frac{1}{2}E_{\text{tot}}[\alpha - U], \tag{3b}$$

where $E_{\text{tot}}[N_2]$ is the total energy of nitrogen molecule while $E_{\text{tot}}[\alpha\text{-U}]$ the total energy of U bulk unit cell containing two atoms. The chemical potentials of N and U, as calculated according to Eqs. (3a) and (3b), represent extreme cases of N (U)-rich conditions [26], i.e., their minimum values were not considered in the present study. The formation energy of N (U) vacancy with respect to the N_2 molecule (or α-U single crystal) and the energy of N (U) isolated atom are closely

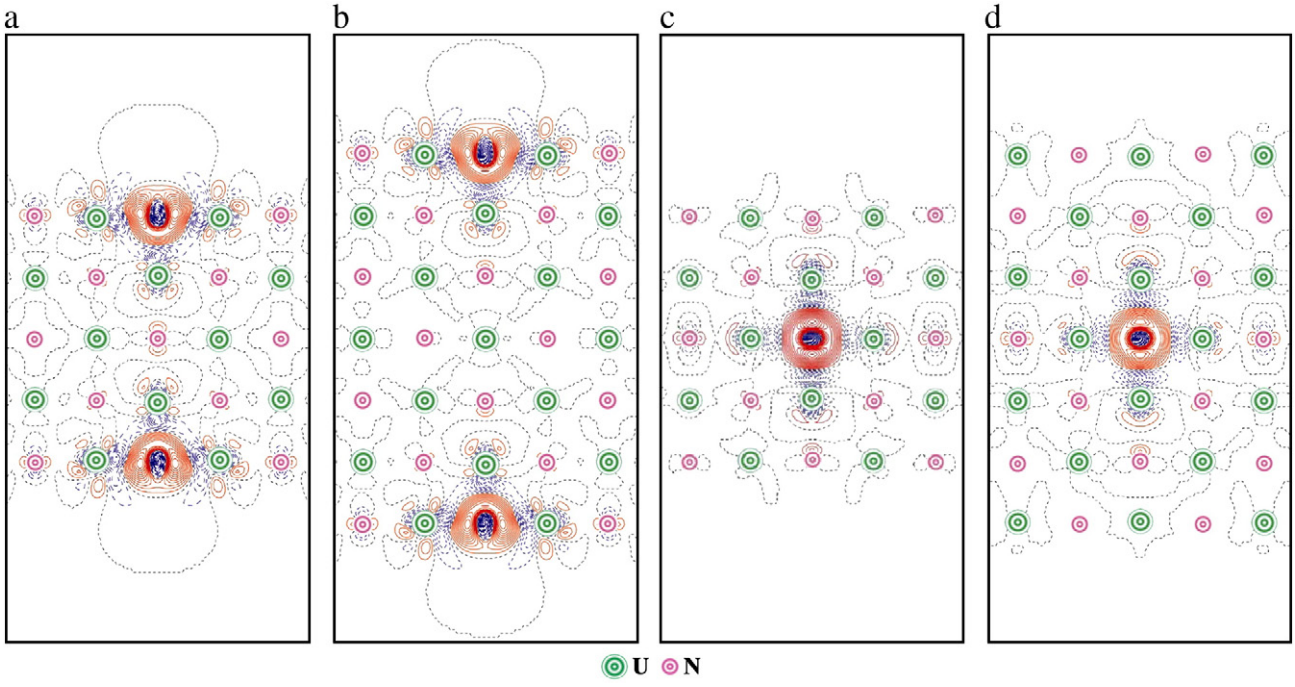

Fig. 3. 2D sections of the electron density redistributions around the nitrogen vacancies in five- and seven-layer UN(001) slabs with 2×2 supercell extension defined as the total electron density of defected surface minus a superposition of the electron densities for both perfect surface and isolated atom in the regular position on the surface: a) N vacancy in a surface plane, five-layer slab, b) the same, 7-layer slab, c) N vacancy in a central plane, five-layer slab, d) the same, 7-layer slab. Solid (red) and dashed (blue) isolines correspond to positive and negative electron density, respectively. Isodensity increment is 0.25 e a.u.$^{-3}$.

related: the former being larger than the latter by half the binding energy of the N_2 molecule or half the cohesive energy of α-U single crystal.

The lattice parameters of α-U were optimized: $a=2.80$ Å, $b=5.88$ Å, $c=4.91$ Å which are slightly underestimated as compared to values obtained experimentally [25] and calculated elsewhere [27,28], except for the parameter b which is in a good agreement with experimental value of 5.87 Å [25] (while $a=2.86$ Å, $c=4.96$ Å [25]). Also, the ratios c/a, b/a as well as the parameter c are well verified by another plane-wave DFT study [29]. Analogously to an isolated nitrogen atom, the N_2 molecule was calculated in the box but of a smaller size ($8\times8\times8$ Å^3). The molecule N_2 is characterized by the bond length of 1.12 Å and the binding energy of 10.63 eV being qualitatively well comparable with the experimental values of 1.10 Å and 9.80 eV [30], respectively.

The formation energies of N and U vacancies ($E_{\text{form}}^{\text{N(U) vac}}$) calculated using Eqs. (1a)–(3b) (with the two reference states as functions of the slab thickness) are collected in Table 4. These are smallest for the surface layer and considerably increase by ~0.6 eV for the N vacancy and by ~1.7 eV for the U vacancy in the sub-surface and central layers, independently of the reference state. This indicates the trend for vacancy segregation at the interfaces (surface or grain boundaries). A weak dependence of $E_{\text{form}}^{\text{N(U) vac}}$ on the slab thickness is also observed. The value of $E_{\text{form}}^{\text{N(U) vac}}$ is saturated with the slab thicknesses of seven atomic layers and more. Moreover, the difference between values of $E_{\text{form}}^{\text{N(U) vac}}$ for the 5 and 7 layer slabs is less for the surface vacancies than for those in the central layer. This difference is the largest for the U vacancy in the central plane (~0.16 eV).

The reference state II leads to smaller $E_{\text{form}}^{\text{N(U) vac}}$ (as compared to those found with the reference state I) and demonstrates a significant difference for two types of vacancies. According to reference II, the U vacancy could be substantially easier formed at $T=0$ K than the N vacancy. Notice that the chemical potentials of O and U atoms used in similar defect studies on UO_2 bulk did not reveal the energetic preference for U vacancy [28,31]. The defect–defect interaction is not responsible for this effect as $E_{\text{form}}^{\text{N(U) vac}}$ decreased by 0.1 eV only with the larger supercell size (3×3 in Table 4). On the other hand, due to the temperature dependence of the chemical potential of a free N_2 molecule [32], we predict reduction of the formation energy of the N vacancy by ~0.8 eV as the temperature increases from RT to 1000 °C. Unlike the reference state II, the reference I results in similar formation energies for both types of the vacancies. In the central slab layer, values of $E_{\text{form}}^{\text{N(U) vac}}$ were found to be similar to those in the bulk (Table 4).

The local atomic displacements around the vacancies are largest for the nearest neighbors of vacancies. The analysis of atomic displacements allows us to suggest that the U vacancy disturbs the structure of the surface stronger than the N vacancy. If the N vacancy lies in the surface layer, displacements of the nearest U atoms in z-direction achieve 0.02–0.05 Å towards the central plane of slab. The displacements of N atom nearest to surface N vacancy achieve 0.05 Å towards the central plane (z-direction) and 0.01 Å in xy (surface) plane. Maximum displacements of neighbor atoms around the N vacancy in the central plane have been found to be 0.04–0.07 Å (nearest U atoms from the neighboring layers are shifted in z-direction towards the vacancy), and do not exceed 0.025 Å for all the other atoms in the slab.

In contrast, the U vacancy results in much larger displacements of neighboring atoms, independently of its position. If the U vacancy is in the surface layer, then the atomic displacements of 0.3–0.32 Å are observed for the nearest N atoms. If the U vacancy lies in the central layer, then the nearest N atoms from this layer are displaced by 0.17 Å, while the N atoms from the nearest layers are not shifted in xy direction, being displaced by 0.15 Å towards the slab surface in the z-direction. Furthermore, the atomic displacements are weakly dependent on the slab thickness. The atomic displacements around the N and U vacancies in the UN bulk have been found to be −0.03 Å and 0.13 Å for N and U vacancies, respectively [15]. These values are close to those found in the present calculations for the vacancies in the central slab layer, which mimics the crystal bulk.

The finite slab-size effects caused by relatively large concentration of defects could be illustrated using the difference electron density redistribution $\Delta\rho(\mathbf{r})$. In Fig. 3, these redistributions are shown for N vacancies positioned at both the outer surface and central (mirror) planes of 5- and 7-layer slabs. Presence of two symmetrically positioned vacancies in the 5-layer slab induces their weak interaction across the slab (Fig. 3a) illustrated by appearance of an additional electron density around the N atoms in the central plane of the slab.

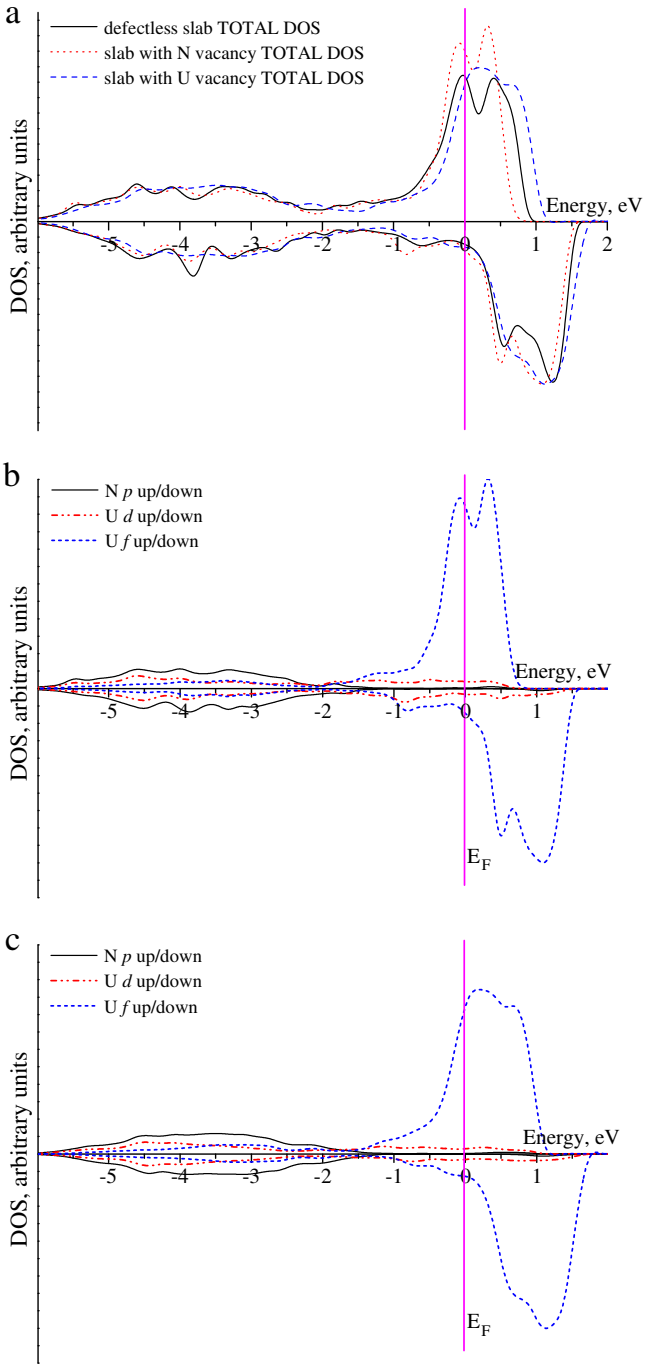

Fig. 4. The total and projected DOSs of 7-layer UN(001) slab (2×2 supercell for vacancy-containing models): a) total DOS of defective and defect-free surfaces, b) projected DOSs for the surface containing N vacancies, c) projected DOSs for the surface containing U vacancies.

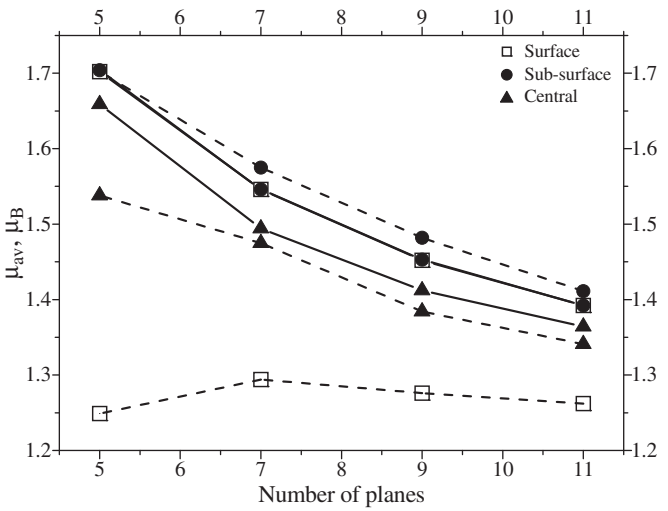

Fig. 5. The average U magnetic moment μ_{av} (in μ_B) in the slab as a function of a number of planes. The dashed curves correspond to U vacancy, whereas the solid curves describe the N vacancy.

Similarly, the vacancy in the mirror plane disturbs the atoms in the surface plane if thin slab contains only 5 layers (Fig. 3c). By increasing the slab thickness, we can avoid the effect of finite slab size (Fig. 3b and d) which explains the stabilization of formation energies calculated for the 7-layer and thicker UN(001) slabs (Table 4).

The densities of states (DOS) are presented in Fig. 4 for perfect and defective 7-layer UN slab. The DOS for other slabs calculated in this study did not demonstrate additional effects and, thus are not shown here. In accordance with previous bulk calculations [10,15], the U(5*f*) electrons occupy the Fermi level (Fig. 4a). These electrons are relatively localized but still strongly hybridized with the N(*2p*) electrons. It confirms the existence of covalent bonding observed in the analysis of Bader charges (Table 2). The N(2*p*) states form a band of the width ~4 eV similar to that obtained in the bulk [10,15]. In contrast, the contribution of U(6*d*) electrons remains insensitive to the presence of vacancies as these are almost homogeneously distributed over a wide energy range including the conduction band.

The analysis of the average magnetic moment of U atoms (μ_{av}^{U}) in the defective UN slabs is done too (Fig. 5). It decreases for both types of vacancies as a function of a number of layers in the slab, except for the U vacancy in the surface layer which remains almost unchanged. On the other hand, μ_{av}^{U} increases significantly when the U vacancy is located in the sub-surface and surface layers. In contrast to the U vacancies, μ_{av}^{U} for the slabs with the N vacancies are less sensitive to the position of defect. Moreover, the values of μ_{av}^{U} for the slabs with the N vacancies in the surface and sub-surface planes are practically identical.

4. Conclusions

In the present study, the basic properties of vacancies on the UN (001) surface were calculated from the first principles. In particular, the formation energies for U and N vacancies were determined using the two reference states, which included the energies of isolated atoms as well as atoms in the metallic α-U phase and N_2 molecule, respectively. The formation energies indicated a clear trend for segregation towards the surface (and probably, grain boundaries) as these energies for surface layer are noticeably smaller than those for sub-surface and central layers (although both latter are very close). However, the magnetic moments in the sub-surface and central layers differ significantly. We demonstrated also a considerable deviation of effective atomic charges from formal charges (caused by a covalent contribution to the U-N chemical bond). The obtained results will be used in the oncoming study of oxygen interaction with real (defective) UN surfaces, in order to understand the atomistic mechanism of UN oxidation.

Acknowledgements

This study was partly supported by the EC FP7 *F-BRIDGE* project and ESF project No.2009/0216/1DP/1.1.1.2.0/09/APIA/VIAA/044. D.B. gratefully acknowledges the doctoral studies support from the European Social Fund (ESF). The authors kindly thank R.A. Evarestov, P. Van Uffelen, and V. Kashcheyevs for fruitful discussions.

References

[1] P.D. Wilson (Ed.), The Nuclear Fuel Cycle, University Press, Oxford, 1996,, www.gen-4.org.
[2] Y. Arai, M. Morihira, T. Ohmichi, J. Nucl. Mater. 202 (1993) 70.
[3] R. Atta-Fynn, A.K. Ray, Phys. Rev. B 76 (2007) 115101.
[4] M.S.S. Brooks, J. Phys. F Metal Phys. 14 (1984) 639.
[5] M. Samsel-Czekała, E. Talik, P. de V. Du Plessis, R. Troć, H. Misiorek, C. Sułkowski, Phys. Rev. B 76 (2007) 144426.
[6] M.S.S. Brooks, D. Glötzel, Physica 102B (1980) 51.
[7] E.A. Kotomin, Yu.A. Mastrikov, Yu.F. Zhukovskii, P. Van Uffelen, V.V. Rondinella, Phys. Stat. Sol. C 4 (2007) 1193.
[8] R.A. Evarestov, M.V. Losev, A.I. Panin, N.S. Mosyagin, A.V. Titov, Phys. Stat. Sol. B 245 (2008) 114.
[9] E.A. Kotomin, Yu.A. Mastrikov, J. Nucl. Mater. 377 (2008) 492.
[10] R.A. Evarestov, A.V. Bandura, M.V. Losev, E.A. Kotomin, Yu.F. Zhukovskii, D. Bocharov, J. Comput. Chem. 29 (2008) 2079.
[11] R. Dovesi, V.R. Saunders, C. Roetti, R. Orlando, C.M. Zicovich-Wilson, F. Pascale, B. Civalleri, K. Doll, N.M. Harrison, I.J. Bush, Ph. D'Arco, M. Llunell, CRYSTAL2006 User's Manual, Universita di Torino, Torino, 2006, http://www.crystal.unito.it/.
[12] G. Kresse, J. Furthmüller, *VASP* the Guide, University of Vienna, 2009, http://cms.mpi.univie.ac.at/vasp/.
[13] Yu.F. Zhukovskii, D. Bocharov, E.A. Kotomin, R.A. Evarestov, A.V. Bandura, Surf. Sci. 603 (2009) 50.
[14] Yu.F. Zhukovskii, D. Bocharov, E.A. Kotomin, J. Nucl. Mater. 393 (2009) 504.
[15] E.A. Kotomin, R.W. Grimes, Yu.A. Mastrikov, N.J. Ashley, J. Phys. Condens. Matter 19 (2007) 106208.
[16] E.A. Kotomin, Yu.A. Mastrikov, S. Rashkeev, P. van Uffelen, J. Nucl. Mater. 393 (2009) 292.
[17] G. Kresse, J. Furthmüller, Comput. Mater. Sci. 6 (1996) 15.
[18] G. Kresse, D. Joubert, Phys. Rev. A 59 (1999) 1758.
[19] J.P. Perdew, J.A. Chevary, S.H. Vosko, K.A. Jackson, M.R. Pederson, D.J. Singh, C. Fiolhais, Phys. Rev. B 46 (1992) 6671.
[20] H.J. Monkhorst, J.D. Pack, Phys. Rev. B 13 (1976) 5188.
[21] M. Methfessel, A.T. Paxton, Phys. Rev. B 40 (1989) 3616.
[22] H.-J. Matzke, Science of Advanced LMFBR Fuels, North Holland, Amsterdam, 1986.
[23] R. Bader, Atoms in molecules: a quantum theory, Oxford University Press, New York, 1990.
[24] G. Henkelman, A. Arnaldsson, H. Jónsson, Comput. Mater. Sci. 36 (2006) 354.
[25] J. Akella, S. Weir, J.M. Wills, P. Söderlind, J. Phys. Condens. Matter 9 (1997) L549.
[26] C.G. Van de Walle, J. Neugebauer, J. Appl. Phys. 95 (2004) 3851.
[27] P. Söderlind, Phys. Rev. B 66 (2002) 085113.
[28] B. Dorado, M. Freyss, G. Martin, Eur. Phys. J. B 69 (2009) 203.
[29] M. Freyss, Phys. Rev. B 81 (2010) 014101.
[30] D.R. Lide (Ed.), CRC Handbook of Chemistry and Physics, 88th Edition, CRC Press, 2007-2008.
[31] M. Iwasawa, Y. Geng, Y. Kaneta, T. Ohnuma, H.-Y. Geng, M. Kinoshita, Mater. Trans. 47 (2006) 014101.
[32] NIST Chemistry Web-book, http://www.webbook.nist.gov/chemistry/2010.

Journal of Nuclear Materials 416 (2011) 200–204

Contents lists available at ScienceDirect

Journal of Nuclear Materials

journal homepage: www.elsevier.com/locate/jnucmat

Ab initio modeling of oxygen impurity atom incorporation into uranium mononitride surface and sub-surface vacancies

D. Bocharov [a,b,c,*], D. Gryaznov [a], Yu.F. Zhukovskii [a], E.A. Kotomin [a]

[a] Institute of Solid State Physics, Kengaraga 8, LV-1063 Riga, Latvia
[b] Faculty of Physics and Mathematics, University of Latvia, Zellu 8, LV-1002 Riga, Latvia
[c] Faculty of Computing, University of Latvia, Raina blvd. 19, LV-1586 Riga, Latvia

ARTICLE INFO

Article history:
Available online 14 December 2010

ABSTRACT

The incorporation of oxygen atoms has been simulated into either nitrogen or uranium vacancy at the UN(0 0 1) surface, sub-surface or central layers. For calculations on the corresponding slab models both the relativistic pseudopotentials and the method of projector augmented-waves (PAW) as implemented in the VASP computer code have been used. The energies of O atom incorporation and solution within the defective UN surface have been calculated and discussed. For different configurations of oxygen ions at vacancies within the UN(0 0 1) slab, the calculated density of states and electronic charge re-distribution was analyzed. Considerable energetic preference of O atom incorporation into the N-vacancy as compared to U-vacancy indicates that the observed oxidation of UN is determined mainly by the interaction of oxygen atoms with the surface and sub-surface N-vacancies resulting in their capture by the vacancies and formation of O–U bonds with the nearest uranium atoms.

1. Introduction

Uranium mononitride (UN) is considered as a promising nuclear fuel for the fast nuclear Generation IV reactors [1]. It has several advantages as compared to the traditional oxide nuclear fuels [2]. The synthesis of UN may be carried out by direct substitution starting from fluorides (*e.g.*, using oxidative ammonolysis of uranium fluorides to uranium nitride [3]). However, oxygen impurities always presented in UN lead to its unwanted pollution and further degradation in air. A number of experiments were performed, in order to understand an influence of oxygen on UN properties and other actinide compounds [4–6]. Various experimental analyses clearly manifested that oxygen contact with the actinide nitride surfaces can result in growth of the oxide [4,5] and, at initial stages, leads to the formation of oxynitrides [6]. The oxynitrides of varying structure (UO_xN_y) can be formed in the reactions of uranium metal with NO_2 [7] or by direct current sputtering upon U target in an Ar atmosphere containing admixture of O_2 and N_2 [8]. This facilitates importance of UO_xN_y for actinide surface studies.

Beginning with 1980s [9,10] a number of *ab initio* calculations on UN bulk [11–16] were performed using formalism of the Density Functional Theory (DFT). It is also worth mentioning that the first-principles calculations on actinide nitride compounds continue attracting great attention, due to improved methods and increasing interest for the fast breeder reactors and for the issues of transmutation of plutonium and minor actinides. Basic bulk properties of actinide nitrides were considered in a few recent studies [17–19], with emphasis on elastic and magnetic properties. The first electronic structure simulations on the perfect UN(0 0 1) *surface* and its reactivity towards the molecular and atomic oxygen were performed only recently [20–22]. These studies clearly show that the O_2 molecule after adsorption on the UN(0 0 1) surface dissociates spontaneously, whereas the newly-produced O atoms demonstrate a strong chemisorption at the surface. For simplicity, we call hereafter O adatoms despite the fact that these are negatively charged ions O^-. Additionally, a considerable attention [14] was paid to the static and dynamic properties of primary defects (vacancies) in UN *bulk* [15] which affect the fuel performance during operation and its reprocessing.

Apart the behavior of empty vacancies, the O atom incorporation into vacancies in bulk UN was considered. Its incorporation into the N-vacancies was found to be energetically more favorable as compared to the interstitial sites [23]. However, the solution energy has shown an opposite effect. The migration energy for the O atom via the interstitial sites along the [0 0 1] direction is 2.84 eV [23,24]. Defective UN surface containing both nitrogen and uranium vacancies disposed at different positions within the UN(0 0 1) slab has been also discussed in a separate paper [25]. In order to shed more light on the mechanism of UN unwanted oxidation, the incorporation of oxygen impurities into the N- and U-vacancies on the UN(0 0 1) surface is focused in this paper.

* Corresponding author at: Institute of Solid State Physics, Kengaraga 8, LV-1063 Riga, Latvia. Fax: +371 67132778.
E-mail address: bocharov@latnet.lv (D. Bocharov).

0022-3115/$ - see front matter © 2010 Elsevier B.V. All rights reserved.
doi:10.1016/j.jnucmat.2010.11.090

2. Computational details

For the simulation of a defective UN(0 0 1) substrate with empty and oxygen-occupied vacancies, the DFT plane wave computer code VASP 4.6 [26–29] was employed. The VASP package is suited for performing first-principles calculations based on the DFT approximation when varying the free energy and evaluating the instantaneous electronic ground state at each quantum-mechanical molecular dynamics time step [26,30]. Ultra-soft pseudopotentials combined with the PAW method [31,32] were used. Computational procedures implemented in this code [26,27] foresee the iterative solution of the Kohn–Sham equations based on both residuum-minimization and optimized charge-density mixing routines [28,29]. The non-local exchange–correlation functional within the Perdew–Wang-91 Generalized Gradient Approximation (PW91 GGA) [33] and the relativistic pseudopotentials for 78 U core electrons (with $6s^2 6p^6 6d^2 5f^2 7s^2$ valence shell), as well as 2 both N and O core electrons (with $2s^2 2p^3$ and $2s^2 2p^4$ valence shells, respectively) were applied in the current study. The Monkhorst–Pack scheme [34] with a $8 \times 8 \times 1$ k-point meshes in the Brillouin zone (BZ) was used while the cut-off energy was set to 520 eV. It became common in last years to use the so-called GGA + U approach to such strongly correlated systems as actinides (*e.g.*, UO_2 [35] and references therein). On the other hand, our test calculations with reasonable U-parameters have shown that the relative variation in the defect formation energies may be ~10% which does not affect main trends and conclusions of the present study. This is why the standard GGA approximation was used which is important for a comparison with previous calculations of defect energies in the UN bulk [15].

For the symmetric UN(0 0 1) substrate possessing the *fcc* rock-salt structure, a slab model was employed. It consists of 5, 7 or 9 atomic layers and containing regularly alternating U and N atoms. The 2D slabs are separated by a vacuum gap of sixteen interlayer distances (38.88 Å) in the z-direction. This inter-slab distance is large enough to exclude the spurious interaction between the slabs. Our calculations supposed the supercells with 2×2 and 3×3 extensions of translation vector for the (0 0 1) surface of UN. Both empty as well as oxygen-occupied N- and U-vacancies were disposed in the surface, sub-surface and central layers of 2D slab. Due to the presence of mirror layers in the symmetric slabs, one can consider the two-sided symmetric arrangement of defects (Fig. 1), except for the central mirror plane, thus, minimizing the computational expenses. Fig. 1 also shows the oxygen-occupied N-vacancies with a 2×2 and 3×3 periodicity disposed on the surface layer. The lattice constant of UN slabs is fixed at 4.87 Å, taken from the lattice relaxation of the UN bulk [20]. In all the calculations, the structural optimization within the supercell of fixed linear dimensions was performed, using the standard procedure of total energy minimization. Our test calculations have shown that the ferromagnetic (FM) phase is energetically slightly more favorable for UN *slabs* than the anti-ferromagnetic (AFM) one. The spin magnetic moment was allowed to relax in all the calculations for the FM spin arrangements on the uranium sub-lattice.

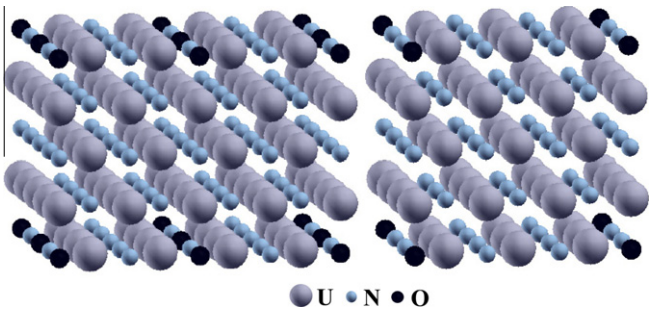

Fig. 1. The symmetrical five-layer UN(0 0 1) slab with a 2×2 (left) and 3×3 (right) periodicity of the oxygen atoms incorporated into the surface N-vacancies.

3. Incorporation and solution energies

The energy balance for the incorporation of an O atom into a vacancy can be characterized by *the incorporation energy* E_I suggested by Grimes and Catlow [36] in the shell model calculations on fission products in UO_2:

$$E_I = E^{N(U)}_{O\_inc} - E^{N(U)}_{vac} - E_O \tag{1a}$$

for the O atom incorporated into the N- and U-vacancy disposed in the central atomic layer and

$$E_I = \frac{1}{2}\left(E^{N(U)}_{O\_inc} - E^{N(U)}_{vac} - 2E_O\right) \tag{1b}$$

for the same incorporation in the surface or sub-surface layers. Here $E^{N(U)}_{O\_inc}$ is the total energy of the supercell containing the O atom at either the N- or U-vacancy $\left(E^{N(U)}_{O\_inc} < 0\right)$, $E^{N(U)}_{vac}$ the energy of the supercell containing an unoccupied (empty) vacancy, and E_O half the total energy of isolated O_2 molecule in the triplet state. It is defined by the oxygen chemical potential at 0 K. Since the value of E_I describes the energy balance for the incorporation into pre-existing vacancies, it has to be negative for energetically favorable incorporation processes.

To take into account the total energy balance, including the vacancy formation energy E_{form} in the defect-free slab, the solution energy [36] was defined as:

$$E_S = E_I + E_{form} \tag{2}$$

where E_{form} is the formation energy of N- or U- vacancy in the slab, calculated as

$$E_{form} = E^{N(U)}_{vac} + E^{N(U)}_{atom} - E^{UN} \tag{3a}$$

for a defect in the central atomic layer of the slab and

$$E_{form} = \frac{1}{2}\left(E^{N(U)}_{vac} + 2E^{N(U)}_{atom} - E^{UN}\right) \tag{3b}$$

for a defect in the surface or sub-surface layer. Here E^{UN} is an energy of the defectless relaxed slab, and $E^{N(U)}_{atom}$ can be defined as chemical potentials of N or U atom, which is, in general, a function of temperature and nitrogen partial pressure. The chemical potential of nitrogen at 0 K is defined by the total energy of N_2 molecule, *i.e.*, $\mu_{N_2} = \frac{1}{2}E_{tot}[N_2]$, while the chemical potential of U atom at 0 K can be estimated as the total energy, *per* atom, for metallic uranium in its low-temperature ortho-rhombic α-phase: $\mu_{\alpha U} = \frac{1}{2}E_{tot}[\alpha U]$. The co-factor of 1/2 in Eqs. (1b) and (3b) as well as multiplication of E_O and $E^{N(U)}_{atom}$ by 2 in the same equations appears due to the symmetric arrangement of incorporated O atoms.

More details on calculations of unoccupied N- and U- vacancies and parameters of calculated of N_2 and α-U are given in Ref. [25]. It is worth mentioning, however, that use of the standard O pseudopotential in our VASP calculations gave good bond length of 1.23 Å for the O_2 molecule but considerable overestimate of the binding energy (6.79 eV *vs.* the experimental value of 5.12 eV). Several corrections were suggested in the literature how to take into account this serious DFT shortcoming [37,38]. Thus, the calculated defect formation and solution energies may be corrected by ~1 eV (its impact is also discussed below).

Table 1
Incorporation (E_I), solution (E_S) energies in eV, average spin magnetic moments of U atoms μ^U_{av} in μ_B and effective charge of O atoms in e^- for O incorporation into the UN(0 0 1) surface. The reference states for calculating the incorporation and solution energies are the chemical potentials of O, N and U calculated for O_2, N_2 molecules and α-U, respectively.

Layer	Supercell size	Number of atomic layers in slab	N-vacancy				U-vacancy			
			E_I (eV)	E_S (eV)	μ^U_{av} (μ_B)	q_{eff} (e^-)	E_I (eV)	E_S (eV)	μ^U_{av} (μ_B)	q_{eff} (e^-)
Surface	2 × 2	5	−6.173	−2.473	1.65	−1.36	−0.339	1.120	1.16	−0.98
		7	−6.181	−2.476	1.49	−1.36	−0.855	0.583	1.36	−1.03
		9	−6.188	−2.479	1.41	−1.36	−0.943	0.493	1.31	−1.06
	3 × 3	5	−6.122	−2.481	1.60	−1.37	−0.683	0.654	1.48	−1.05
		7	−6.126	−2.480	1.46	−1.36	−1.073	0.230	1.38	−1.08
Sub-surface	2 × 2	5	−6.314	−2.068	1.64	−1.42	−1.856	1.284	1.66	−1.10
		7	−6.419	−2.090	1.49	−1.40	−1.823	1.297	1.45	−1.10
		9	−6.417	−2.091	1.41	−1.40	−1.823	1.271	1.38	−1.10
	3 × 3	7	−6.428	−2.093	1.46	−1.39	−2.012	1.000	1.43	−1.10
Central (mirror)	2 × 2	7	−6.611	−2.180	1.47	−1.42	0.736	3.923	1.44	−0.89
		9	−6.608	−2.192	1.39	−1.38	0.669	3.838	1.38	−0.90
	3 × 3	7	−6.599	−2.182	1.45	−1.42	0.317	3.378	1.47	−0.94

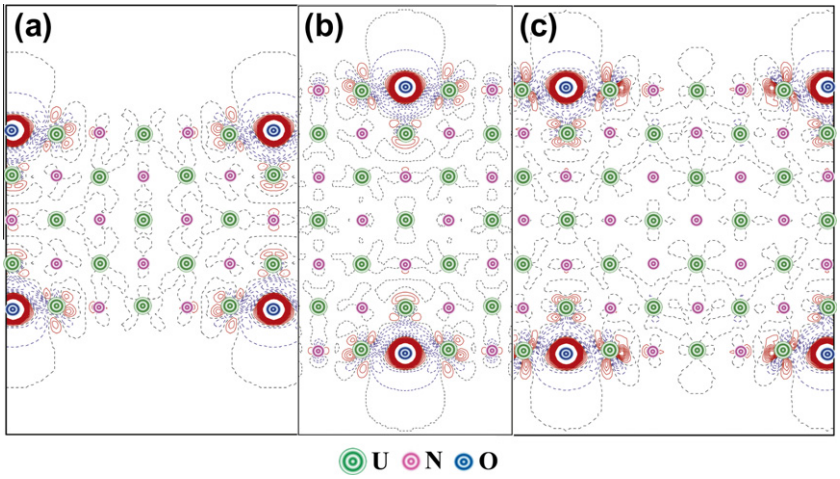

Fig. 2. The 2D sections of the electron charge density redistributions $\Delta\rho(\mathbf{r})$ around the O atoms incorporated into the surface N-vacancies of the five- and seven-layer UN(0 0 1) slabs with 2 × 2 and 3 × 3 supercell extensions. $\Delta\rho(\mathbf{r})$ are defined as the total electron density of the O-containing defected surface minus a superposition of the electron densities of the surface containing the N-vacancies and the O atom in the regular positions on the surface. (a) 3 × 3 periodicity of the oxygen atoms upon the five-layer slab, (b) 2 × 2 periodicity of the oxygen atoms upon the seven-layer slab, (c) 3 × 3 periodicity of the oxygen atoms upon the seven-layer slab. Solid (red) and dashed (blue) isolines correspond to positive and negative electron density, respectively. Dashed black isolines correspond to the zero-level. Isodensity increment is 0.25 e a.u.$^{-3}$. (For interpretation of the references to colour in this figure legend, the reader is referred to the web version of this article.)

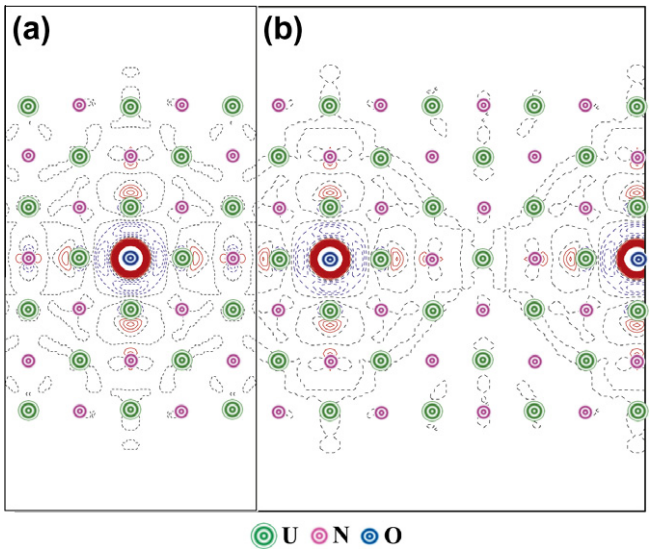

Fig. 3. The 2D sections of $\Delta\rho(\mathbf{r})$ around the O atoms incorporated into the N-vacancies disposed in central layer of the seven-layer UN(0 0 1) slabs with (a) 2 × 2 and (b) 3 × 3 supercell extensions. Other details are given in caption of Fig. 2.

4. Results and discussion

The calculated O atom incorporation into the N-vacancies at the UN(0 0 1) surface is energetically favorable since both values of E_I and E_S are strictly negative (Table 1), thus, being in favor of both creating the N-vacancy and adsorbing the O atom from air. Also, E_I decreases by ∼0.4 eV (becomes more negative) within the slab as compared to the surface layer, whereas E_S is smallest for the N-vacancy just on the surface layer. Contrary, in case of the U-vacancies, the values of E_I calculated for the surface and central layers are found to be close to zero. The sub-surface layer is characterized by E_I which is ∼1 eV smaller than that for the surface and central layers. Our results indicate importance of oxynitride formation. However, E_S is positive and increases for O atoms in the the U-vacancy and the slab centre. Note that the energies in Table 1 do not include the corrections discussed above for the O atoms. However, such corrections may lead to E_I (or E_S) increased by ∼1 eV and, as a result, more positive E_I for the U-vacancy. Table 1 also indicates that solution of the oxygen atoms is energetically more favorable at the surface layers than in the slab. As the supercell size increases (the 3 × 3 extension in Table 1), both E_I and E_S values decrease whereas the slab thickness has no such clear effect. Nevertheless, the U-vacancy appeared to be most sensitive to the

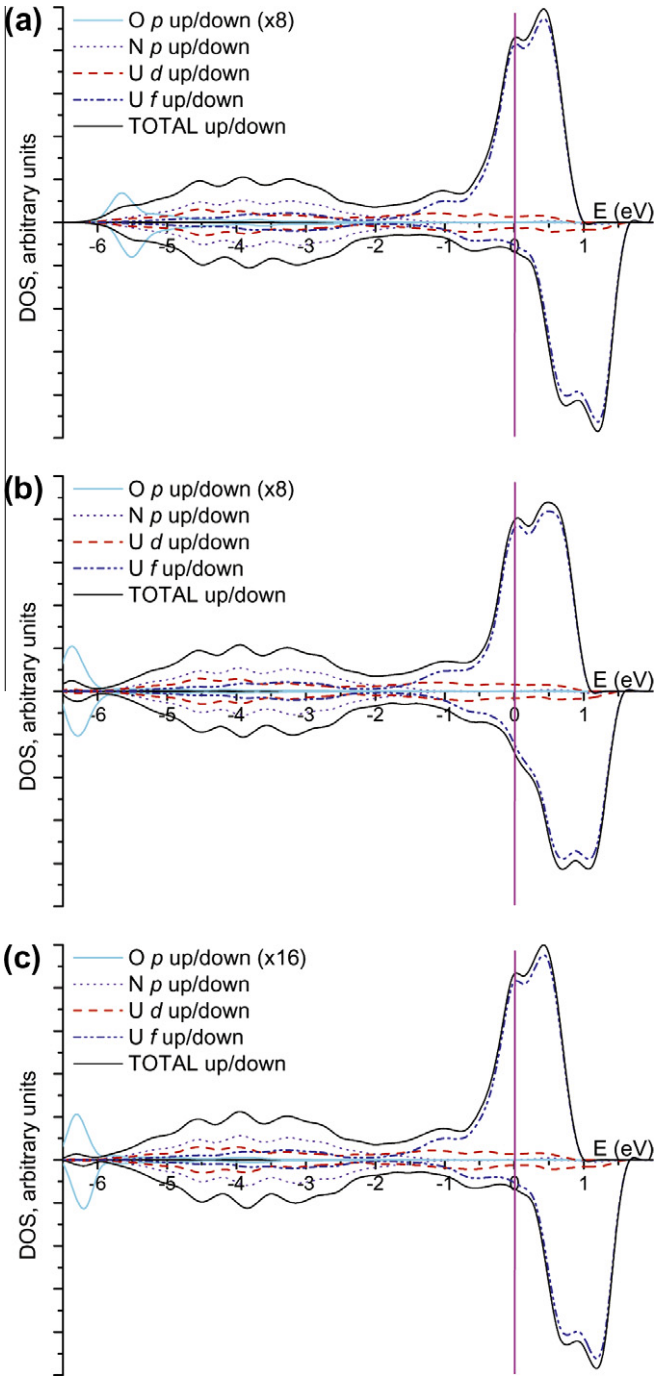

Fig. 4. The total and projected DOS for three positions of O atoms incorporated into the N-vacancies with a 3×3 periodicity across the seven-layer UN(0 0 1) slab: (a) surface layer, (b) sub-surface layer, (c) central layer. The O 2*p* peaks have been normalized to the same value, *i.e.*, these were multiplied by a factor of 8 and 16 for vacancies in the surface (sub-surface) and central layers, respectively (please see figure labels), A convolution of individual energy levels has been plotted using the Gaussian functions with a half-width of 0.2 eV.

supercell size which is related to spurious interactions between the periodically repeated defects. The E_I as well as E_S values may be reduced by 0.15 eV at the average in this case.

Table 1 allows us to analyze also the averaged spin density of U atoms μ_{av}^{U} for different morphologies of defective UN(0 0 1) surfaces with incorporated O atoms. Analogously to defective UN surface with empty vacancies [25], μ_{av}^{U} decreases with a number of layers in the slab for both types of the vacancies (except for the O atom incorporated into the U-vacancy in the surface layer). It is also seen that μ_{av}^{U} is higher in the surface layer for the N-vacancy than for the U-vacancy. The sub-surface and central layers are characterized by similar μ_{av}^{U} for both the vacancies. Interestingly, the effective charge q_{eff} of O atoms is also higher for the N-vacancy and inside the slab. In the case of U-vacancy, however, q_{eff} decreases by almost 0.3 e. The same effect is also seen for the N atoms their effective charge is smaller when the O atom occupies the U-vacancy (not shown here). The overall picture suggests prevalence of the covalent bonding between different species in the system.

Large concentrations of defects (25% for the 2×2 extension in Table 1) causes certain finite-size effects which can be illustrated using the 2D difference electron density redistributions $\Delta\rho(\mathbf{r})$. These redistributions are shown for the O atoms incorporated into the N-vacancies at the surface (Fig. 2) and central layers (Fig. 3). Inside the five-layer slab, a presence of the two symmetrically positioned defects induces their interaction (visible in charge redistribution across a slab in Fig. 2a). An increase of the slab thickness reduces this effect (Fig. 2c). If the supercell size is decreased (the 2×2 extension, Fig. 2b) an additional electron density parallel to the surface layer is observed between the defects. Similar effects are also observed for redistributions of the electron density around defects in the mirror planes (Fig. 3). A perfect spherical negative charge redistribution is observed around the O atom in the U-vacancy in the central plane (not shown here). The effect of supercell size in this case is similar to that discussed for the N-vacancy. However, in the case of surface vacancy more electron density is seen between the O atom and neighbouring N atoms in the sub-surface layer, in a comparison to the N-vacancy. Thus, the effect of slab thickness also may not be underestimated in this case.

In Fig. 4, the total and projected density of states (DOS) is shown for the seven-layer defective UN(0 0 1) surface with the O atom incorporated into the N-vacancy. The system remains conducting throughout all the calculations with the significant contribution from the U 5*f* states at the Fermi level similar to pure UN bulk [20]. The appearance of the specific O 2*p* band with the energy peak at −6 eV is observed. When comparing the DOS for the O atoms incorporated into the N–vacancies, a noticeable shift of the O 2*p* band (by about −1.0 eV) allows one to distinguish the surface layer from the internal layers. Moreover, in the case of the surface layer, this band considerably overlaps with the N 2*p* band, partly mixed with the U 5*f* states (similar effects happen with the O_2 molecule atop the surface U atom [22]). Contrary, the O 2*p* band remains quasi-isolated from the other bands (analogously to the O atom incorporated into the N-vacancy in UN bulk [23]). Note that position of the N 2*p* band is insensitive to the presence of O atoms and lies within energy range of −6 and −1 eV.

5. Conclusions

Summing up the results obtained in this and our recent studies, the following stages for reactivity of oxygen positioned atop the UN(0 0 1) surface could be suggested: (i) spontaneous breaking of the O_2 chemical bond after molecular adsorption [22], (ii) location of the two newly formed O adatoms atop the surface U atoms [21], (iii) incorporation of O adatoms in pre-existing surface N-vacancies (as a result of vacancy surface diffusion), (iv) incorporation of O atoms in existing sub-surface N-vacancies as a result of inter-lattice diffusion. This explains an easy UN oxidation observed in air.

The formation of oxynitrides [8] near the UN(0 0 1) surface is proposed, which can be caused by diffusion of the oxygen atoms within the interlayers of uranium nitride with further capture by nitrogen vacancies, thus, resulting in their stabilization due to formation of the chemical bonds with the nearest uranium atoms. The relevant effects of the electronic charge re-distribution were ana-

lyzed. They demonstrate a quite local nature of the density perturbation caused by the incorporated O atoms. The analysis of density of states shows both overlapping of the O 2*p* states with the N 2*p* states at initial stages of oxidation (*surface incorporation*) and separation of the O 2*p* states from other bands in the case of deeper positioned oxygen atoms (*sub-surface penetration*). The results of this analysis could be used for the interpretation of the experimental ultraviolet photoelectron spectra for uranium oxynitrides [8].

Acknowledgements

This study was partly supported by the European Commission FP7 Project *F*-BRIDGE and ESF Project No. 2009/0216/1DP/1.1.1.2.0/09/APIA/VIAA/044. The corresponding author gratefully acknowledges also the doctoral studies support by the European Social Fund. The authors kindly thank R.A. Evarestov, P. Van Uffelen and V. Kashcheyevs for a numerous fruitful discussions. The technical assistance of A. Gopejenko and A. Kuzmin was the most valuable.

References

[1] P.D. Wilson (Ed.), The Nuclear Fuel Cycle, University Press, Oxford, 1996.
[2] B.J. Jaques, B.M. Marx, A.S. Hamdy, D.P. Butt, J. Nucl. Mater. 381 (2008) 309.
[3] C.B. Yeamans, G.W. Chinthaka Silva, G.S. Cerefice, K.R. Czerwinski, T. Hartmann, A.K. Burrell, A.P. Sattelberger, J. Nucl. Mater. 374 (2008) 75.
[4] Y. Arai, M. Morihira, T. Ohmichi, J. Nucl. Mater. 202 (1993) 70.
[5] H. Wiame, M. Centeno, S. Pacard, P. Bastian, P. Grange, J. Eur. Ceram. Soc. 18 (1998) 1293.
[6] G.P. Novoselov, V.V. Kushnikov, V.A. Baronov, V.P. Serebryakov, N.M. Stepennova, Atom. Energy 53 (1982) 528.
[7] A.F. Carley, P. Nevitt, P. Roussel, J. Alloys Compd. 448 (2008) 355.
[8] M. Eckle, T. Gouder, J. Alloys Compd. 374 (2004) 261.
[9] P. Weinberger, C.P. Mallett, R. Podloucky, A. Neckel, J. Phys. C: Solid State Phys. 13 (1980) 173.
[10] M.S. Brooks, J. Phys. F: Metal Phys. 14 (1984) 639.
[11] D. Sedmidubsky, R.J.M. Konings, P. Novak, J. Nucl. Mater. 344 (2005) 40.
[12] Z. Yongbin, M. Daqiao, Z. Zhenghe, M. Meizhong, Chin. J. Chem. Phys. 18 (2005) 735.
[13] E.A. Kotomin, Yu.A. Mastrikov, Yu.F. Zhukovskii, P. Van Uffelen, V.V. Rondinella, Phys. Status Solidi C 4 (2007) 1193.
[14] R. Atta-Fynn, A.K. Ray, Phys. Rev. B 76 (2007) 115101.
[15] E.A. Kotomin, R.W. Grimes, Yu.A. Mastrikov, N.J. Ashley, J. Phys.: Condens. Matter 19 (2007) 106208.
[16] M. Samsel-Czekała, E. Talik, P.deV. Du Plessis, R. Troć, H. Misiorek, C. Sułkowski, Phys. Rev. B 76 (2007) 144426.
[17] H. Shibata, T. Tsuru, M. Hirata, Y. Kaji, J. Nucl. Mater. 401 (2010) 113.
[18] P.F. Weck, E. Kim, N. Balakrishnan, F. Poineau, C.B. Yeamans, K.R. Czerwinski, Chem. Phys. Lett. 443 (2007) 82.
[19] L. Petit, A. Svane, Z. Szotek, W.M. Temmerman, G.M. Stocks, Phys. Rev. B 80 (2009) 045124.
[20] R.A. Evarestov, A.V. Bandura, M.V. Losev, E.A. Kotomin, Yu.F. Zhukovskii, D. Bocharov, J. Comput. Chem. 29 (2008) 2079.
[21] Yu.F. Zhukovskii, D. Bocharov, E.A. Kotomin, R.A. Evarestov, A.V. Bandura, Surf. Sci. 603 (2009) 50.
[22] Yu.F. Zhukovskii, D. Bocharov, E.A. Kotomin, J. Nucl. Mater. 393 (2009) 504.
[23] E.A. Kotomin, Yu.A. Mastrikov, J. Nucl. Mater. 377 (2008) 492.
[24] E.A. Kotomin, D. Gryaznov, R.W. Grimes, D. Parfitt, Yu.F. Zhukovskii, Yu.A. Mastrikov, P. Van Uffelen, V.V. Rondinella, R.J.M. Konings, Nucl. Instrum. Method B 266 (2008) 2671.
[25] D. Bocharov, D. Gryaznov, Yu. F. Zhukovskii, E.A. Kotomin, Surf. Sci., in press, doi:10.1016/j.susc.2010.11.007.
[26] G. Kresse, J. Furthmüller, VASP the Guide, University of Vienna (2009). <http://www.cms.mpi.univie.ac.at/vasp/>.
[27] (a) G. Kresse, J. Hafner, Phys. Rev. B 48 (1993) 13115;
(b) G. Kresse, J. Hafner, Phys. Rev. B 49 (1994) 14251.
[28] G. Kresse, J. Furthmüller, Comput. Mater. Sci. 6 (1996) 15.
[29] G. Kresse, J. Furthmüller, Phys. Rev. B 54 (1996) 11169.
[30] J. Hafner, Comput. Phys. Commun. 177 (2007) 6.
[31] P.E. Bloechl, Phys. Rev. B 50 (1994) 17953.
[32] G. Kresse, D. Joubert, Phys. Rev. B 59 (1999) 1758.
[33] J.P. Perdew, J.A. Chevary, S.H. Vosko, K.A. Jackson, M.R. Pederson, D.J. Singh, C. Fiolhais, Phys. Rev. B 46 (1992) 6671.
[34] H.J. Monkhorst, J.D. Pack, Phys. Rev. B 13 (1976) 5188.
[35] D. Gryaznov, E. Heifets, E. Kotomin, Phys. Chem. Chem. Phys. 11 (2009) 7241.
[36] R.W. Grimes, C.R.A. Catlow, Phil. Trans. Roy. Soc. A 335 (1991) 609.
[37] Y.-L. Lee, J. Kleis, J. Rossmeisl, D. Morgan, Phys. Rev. B 80 (2009) 224101.
[38] Yu. Mastrikov, R. Merkle, E. Heifets, E.A. Kotomin, J. Maier, J. Phys. Chem. C 114 (2010) 3017.